This is the Pre-Published Version.

The following publication Wong, W.-Y., Chau, N.-Y., Wang, Q., Jiang, L., Li, J., & Ma, D. (2024). Highly efficient iridium(iii) phosphors with a 2-(4-benzylphenyl)pyridine-type ligand and their high-performance organic light-emitting diodes [10.1039/D4TC02427C]. Journal of Materials Chemistry C, 12(36), 14485-14495 is available at https://doi.org/10.1039/D4TC02427C.

Highly efficient iridium(III) phosphors with 2-(4-benzylphenyl)pyridine-type ligand and their high-performance organic light-emitting diodes

Wai-Yeung Wong,*[abcd] Nga-Yuen Chau,[d] Qiwei Wang,[ad] Lu Jiang,[a] Junlong Li[a] and Dongge Ma*[e]

[a] *Antibiotics Research and Reevaluation Key Laboratory of Sichuan Province, Sichuan Industrial Institute of Antibiotics, Chengdu University, Chengdu 610052, P. R. China*

[b] *Department of Applied Biology and Chemical Technology, The Hong Kong Polytechnic University, Hung Hom, Hong Kong, P. R. China. E-mail: wai-yeung.wong@polyu.edu.hk*

[c] *The Hong Kong Polytechnic University Shenzhen Research Institute, Shenzhen 518057, P. R. China*

[d] *Department of Chemistry and Institute of Advanced Materials, Hong Kong Baptist University, Waterloo Road, Kowloon Tong, Hong Kong, P. R. China*

[e] *State Key Laboratory of Luminescent Materials and Devices, Center for Aggregation-Induced Emission, South China University of Technology, Guangzhou 510640, P. R. China. E-mail: msdgma@scut.edu.cn*

Abstract

A series of new cyclometalated iridium(III) complexes containing a methyl or trifluoromethyl substituted 2-(4-benzylphenyl)pyridine molecular framework have been synthesized and characterized. All these complexes are amorphous and possess excellent thermal stabilities. Arising from the propensity of the tetrahedral geometry of the CH_2 moiety in the benzyl group, this could make the metal complexes less crystalline, attain more morphologically stable thin-film formation and reduce the triplet-triplet annihilation process, especially in the solid state. The optical, electrochemical, photo- and electrophosphorescence traits of these iridium(III) phosphors have been studied in terms of the electronic nature of the pyridyl ring substituents. Electrophosphoresent organic light-emitting diodes (OLEDs) with attractive device performance can be fabricated based on these materials. The best electroluminescent (EL) performance can be obtained with a maximum current efficiency (η_L) of 76.3 cd A^{-1}, a maximum power efficiency (η_P) of 51.1 lm W^{-1}, a maximum external quantum efficiency (η_{ext}) of 21.4% and a pure green color of CIE of (0.27, 0.64). The present work provides a simple way to enhance the OLED performance by simply modifying the molecular design of the benchmark emitters, which have great potential for application in multicolor displays.

Introduction

Organic light-emitting diodes (OLEDs) based on phosphorescent emitters have aroused great interest in the scientific and commercial communities owing to their promising applications in full-color displays and low-cost solid state lighting.[1] As the phosphorescent materials can harness both singlet and triplet excitons for emission, they enable OLEDs to achieve an internal quantum efficiency as high as 100% theoretically.[2] The third-row transition metal complexes like Re(I), Os(II), Ir(III) and Pt(II) molecules are well-known phosphorescent emitters and their high spin-orbit coupling constants are capable of facilitating the triplet emission even at room temperature.[3]

Along this line of frontier science, many researchers have studied numerous substituted 2-phenylpyridine (ppy) based iridium(III) complexes as they show tunable emission colors and high phosphorescence quantum yields.[4] Their colors could be fine-tuned by changing the degree of conjugation or modifying the inductive electronic effect of different substituents on the ppy ring, which provide a diverse measure for electrons in the MLCT transition to alter the energy of MLCT states.[5] A very versatile avenue for the emission color switching of Ir(III) complexes via the facile derivatization of the phenyl moiety of ppy with various main group moieties such as $B(Mes)_2$, $SiPh_3$, $GePh_3$, NPh_2, $POPh_2$, OPh and SPh has been demonstrated

previously. [6] Smart design of the ligand structure not only endows the Ir(III) complex with specific color versatility, but also inhibits its aggregation properties, especially in the solid state. In this study, simple tailoring of the phenyl ring of ppy on Ir(III) phosphors by introducing weakly electron-donating CH_2Ph benzyl group have been carried out. Such modified ppy ligand could be utilized to keep high phosphorescence quantum yield relative to *fac*-Ir(ppy)$_3$. On the grounds that the benzyl group could make the metal complexes less crystalline and reduce the likelihood of aggregation-caused quenching in their solid state, their thin-film morphology could then be improved by suppressing the triplet-triplet annihilation which subsequently enhance the OLED device performance. In addition, the CH_2 spacer on ppy effectively acts as the electronic conjugation interrupter, which do not exert any effect on shifting the emission wavelength.[3d] However, their photophysical, electrochemical and electroluminescent properties can be influenced by attaching the electron-donating group (-CH_3) or electron-withdrawing group (-CF_3) into the pyridyl ring of the cyclometalating ligands, which would influence the triplet energy of the phosphor, leading to switchable color. Complexes bearing CF_3 unit on the pyridine ring show red shifts in their emission color.[7] It is observed that incorporating the electron-donating 5-methyl substituent on the pyridyl ring of the ligand results in highly-efficient OLED performance in either the homoleptic or heteroleptic series.

This simple synthetically versatile strategy provides an easy access to OLED efficiency enhancement, essential for highly efficient and multicolor OLEDs.

Results and discussion

A series of 2-(4-benzylphenyl)pyridine-based cyclometalating ligands **L1**–**L5** were first synthesized according to the synthetic protocol as outlined in Scheme 1. Phenylboronic acid derivatives reacted with commercially available 4-bromobenzyl bromide to obtain the corresponding bromides.[8] They were then converted into boronic acids after further reacting with *n*-butyllithium and trimethylborate. **L1**–**L5** were subsequently prepared from the palladium-catalyzed Suzuki-Miyaura coupling of functionalized 4-benzylphenylboronic acid with pyridine, 2-chloro-4-methylpyridine, 2-chloro-5-methylpyridine or 2-chloro-5-trifluoromethylpyridine. Through a one-step cyclometalation, the homoleptic complexes **1**–**4** were easily synthesized by refluxing the corresponding ligands with $[Ir(acac)_3]$ (Hacac = acetylacetone) in glycerol at high temperature (> 200 ^{o}C) (Scheme 2). In this case, the reaction was carried out with an excess of ligand, which can be easily recovered and reused. On the other hand, heteroleptic Ir(III) complexes **5**–**9** were prepared in two steps: the corresponding ligands first reacted with iridium trichloride hydrate to yield the iridium-μ-chloro-bridged dimers. These diiridium(III) complexes were then readily cleaved to mononuclear iridium(III)

complexes **5**–**9** by replacing the bridging chloride with bidentate monoanionic acetylacetonate (acac) ligand. All these complexes were purified by column chromatography on silica gel and then fully structurally characterized by ^{1}H and ^{13}C NMR spectroscopy and MALDI-TOF mass spectrometry. For *tris*-cyclometalated homoleptic Ir(III) complexes, their *facial* geometry has been confirmed in their ^{1}H NMR spectra since only one set of proton signals was revealed, which indicates that the number of coupled spins is equal to that of the protons on one ligand because the three ligands are magnetically equivalent owing to the threefold symmetry of the molecule. The singlet peak at around $\delta = 4.0$ was characteristic of the two protons from the benzylphenyl group in the ligand in each of the metal complexes.

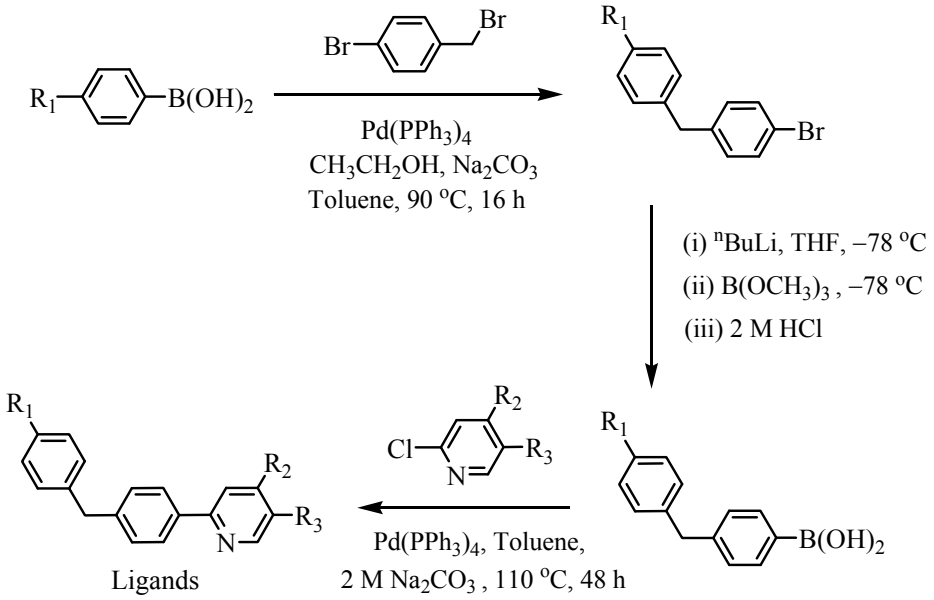

L1: $R_1 = H$, $R_2 = H$, $R_3 = H$; **L2**: $R_1 = CH_3$, $R_2 = H$, $R_3 = H$; **L3**: $R_1 = H$, $R_2 = CH_3$, $R_3 = H$; **L4**: $R_1 = H$, $R_2 = H$, $R_3 = CH_3$; **L5**: $R_1 = H$, $R_2 = H$, $R_3 = CF_3$

Scheme 1 Synthetic route of cyclometalating ligands **L1**–**L5**.

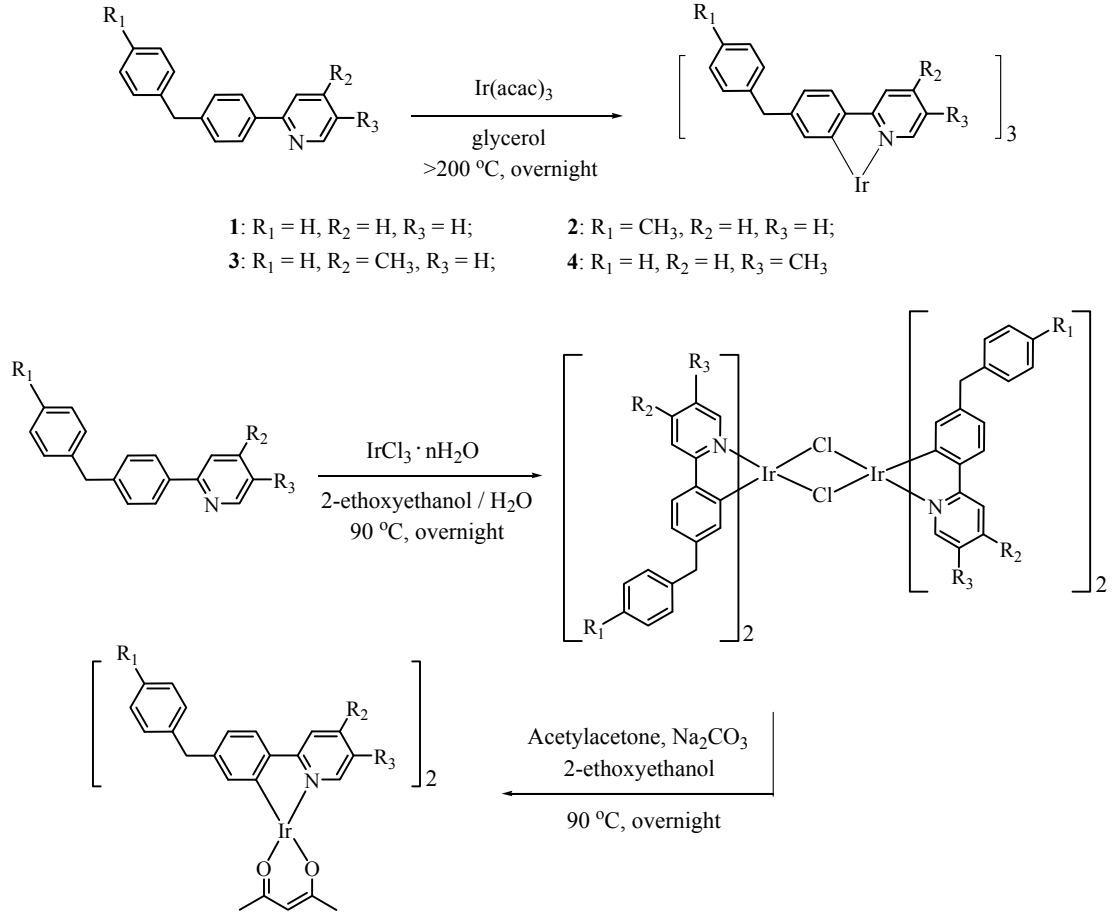

1: R_1 = H, R_2 = H, R_3 = H; **2**: R_1 = CH_3, R_2 = H, R_3 = H;
3: R_1 = H, R_2 = CH_3, R_3 = H; **4**: R_1 = H, R_2 = H, R_3 = CH_3

5: R_1 = H, R_2 = H, R_3 = H; **6**: R_1 = CH_3, R_2 = H, R_3 = H; **7**: R_1 = H, R_2 = CH_3, R_3 = H;
8: R_1 = H, R_2 = H, R_3 = CH_3; **9**: R_1 = H, R_2 = H, R_3 = CF_3

Scheme 2 Synthetic routes of new cyclometalated Ir(III) complexes **1**–**9**.

The thermal stability of the iridophosphors is crucial in OLED applications. The onset decomposition temperatures (T_{dec}) of these phosphors were examined using thermogravimetric analysis (TGA) under a nitrogen stream. All of the new iridium(III) phosphors are thermally stable (405–418 °C for homoleptic series and 309–342 °C for heteroleptic series), which is beneficial for the long-term stability of

OLED devices fabricated from these emitters. The temperatures that induce a 5% weight reduction are notably different between homoleptic and heteroleptic complexes. These results indicate that the complexes with the acac ligand tend to thermally decompose at relatively lower temperatures but are still sufficiently stable enough for sublimation in vacuum-evaporated OLED fabrication without decomposition. Analysis of the differential scanning calorimetry (DSC) traces for **1–9** revealed that these complexes were amorphous materials. They showed no crystallization and melting peaks but only glass-transition temperatures (T_g), which can be attributed to the flexible branched and twisted configuration of the substituted benzyl group despite the relatively small ligand size of the complexes (Table 1). This would prevent molecules from stacking and induce morphologically stable amorphous thin-film formation, leading to improvement of thermal stability and good performance of EL devices.

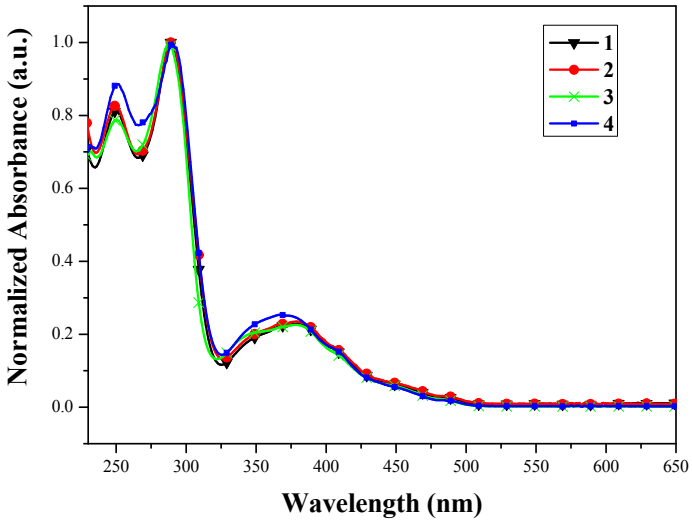

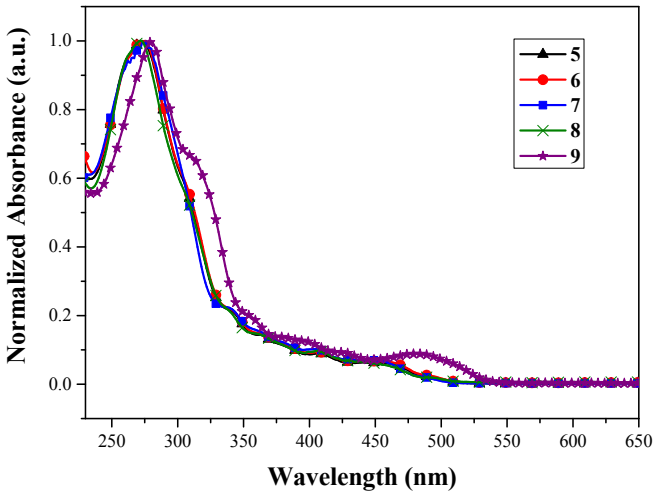

Fig. 1 UV-Vis absorption spectra of complexes **1–9** in CH_2Cl_2 at 298 K.

The UV-Vis absorption and photoluminescence spectra of the complexes were performed in dichloromethane solution and the data are summarized in Table 1. As depicted in the absorption spectra in Fig. 1, the intense bands in the UV region were generally assigned to the ligand-centered π-π* transition that closely resemble the spectra of their corresponding ligands. While the absorption bands at lower energies were mainly attributed to the admixture of the typical spin-allowed metal-to-ligand charge transfer ^{1}MLCT and spin-forbidden ^{3}MLCT, which is caused by the strong spin-orbit coupling due to the heavy metal atom effect. These assignments are made by analogy with the previously reported iridium(III) complexes.[9] By introducing the CF_3 moiety on the pyridyl ring in **9**, there is a significant difference in the energy of the absorption spectrum. The 5-trifluoromethyl-substituted pyridyl ligand in **9** can stabilize the triplet excited state, thereby red-shifting its absorption band with respect

to **5**.

All complexes **1**–**9** are highly phosphorescent in solution at room temperature (298 K) (Fig. 2) as well as in the rigid condition (77 K). The broad and featureless bands of their emission spectra at room temperature convince the predominant MLCT character for their emissive lowest triplet excited states (T_1) with less $^3\pi$-π character. This is commonly observed with Ir(III) complexes that bear small cyclometalating ligands.[10] Different color was emitted upon photoexcitation depending on the nature and position of the substituents on the cyclometalating ligand. For complexes **1**, **2**, **5** and **6**, they are all strongly luminescent with a bright green color. Adding a methyl substituent (R_1) on the benzyl ring in the cyclometalating ligand does not show any influence on the spectral feature in terms of peak emission wavelength, which may plausibly be caused by the blocking of electron conjugation from the CH_2 group. For the corresponding geometrical isomers (**3**–**4** and **7**–**8**, respectively) of **2** and **6**, we note a greater substituent effect on the emission peak position by attaching an electron-donating methyl group to the pyridine ring. The methyl group located *para* or *meta* to the nitrogen atom coordinated to the metal center in **3**–**4** and **7**–**8** show a clear spectral blue-shift. This can be attributed to the notion that an electron-donating group on pyridine would increase the LUMO energy and subsequently enlarge the HOMO-LUMO gap. On the other hand, the incorporation of bulky and inductively

electron-withdrawing CF_3 group into the pyridyl ring of **9** would tend to lower the LUMO energy and thereby decrease the energy gap and emission energy of the emitting excited state.[11] By virtue of the higher ligand field strength of acac anion, the emission peak maxima of heteroleptic complexes **5**–**8** were slightly red-shifted from those of the homoleptic series **1**–**4**.[12] By comparing the CH_2-bridged ligand with the corresponding Si- and Ge-analogues, compound **5** emits at a shorter wavelength (514 nm versus 535 nm for Si and 530 nm for Ge) together with a shorter phosphorescence lifetimes (0.78 μs versus 2.44 μs for Si and 2.17 μs for Ge).[6]

Upon cooling to 77 K, all of the complexes are also intensely luminescent in glassy matrices. The emission spectra of these complexes revealed more vibronic features at higher energies, owing to the effective mixing between the ^{3}MLCT and $^3\pi$–π^* levels so that the ligand-centered emission predominates upon freezing the matrix.[13] All complexes in the solid matrix show rigidochromic blue-shift in emission as compared to that recorded at 298 K. The hypsochromic shifts of the peak maximum are caused by solvent reorganization in a fluid solution at room temperature, which stabilizes the charge-transfer states prior to emission. The process is significantly impeded in a rigid matrix at 77 K, and therefore, emission occurs at a higher energy. Their phosphorescence quantum yields (Φ_p) were measured in degassed CH_2Cl_2 solution at room temperature, using *fac*-Ir(ppy)$_3$ excited at 400 nm

as standard (Φ_p = 0.40). Most of the complexes exhibit relatively high Φ_p (Φ_p = 0.27–0.39). Among all these compounds, complex **4** has the highest Φ_p of 0.39. In addition, their excited-state lifetime measurement was performed in CH_2Cl_2. These highly emitting Ir(III) complexes have short lifetimes (τ_p) of the triplet state in the sub-microsecond range. These data are indicative of strong spin-orbit coupling, leading to effective intersystem crossing from the singlet to the triplet state.[14] It is believed that the phosphorescence lifetime has a great influence on triplet-triplet annihilation in OLED applications.[15]

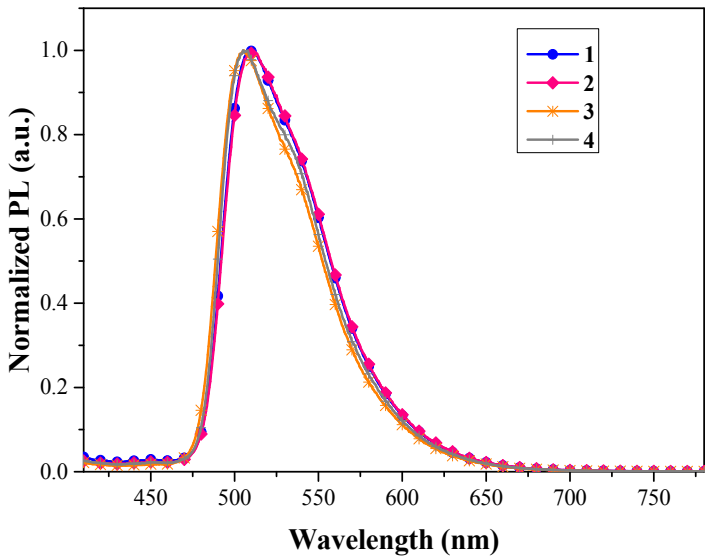

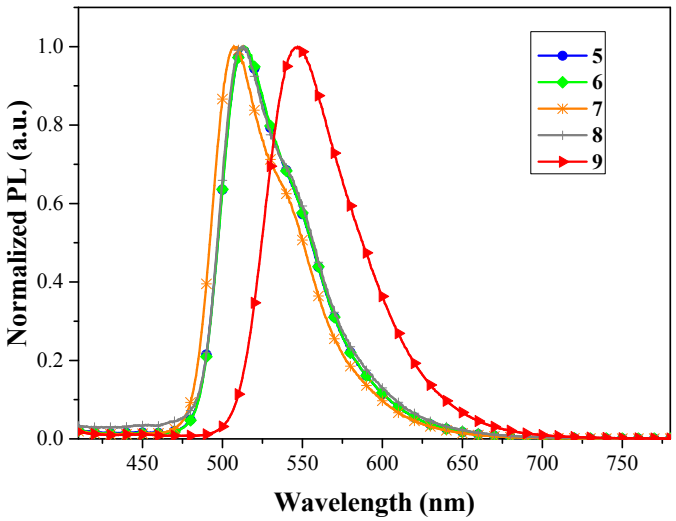

Fig. 2 PL emission spectra of complexes **1–9** in CH_2Cl_2 at 298 K.

Table 1 Photophysical and thermal data for the phosphors **1–9**

	λ_{max} (nm)[a]	λ_{em} [nm] (298 K) [a]	λ_{em} [nm] (77 K) [b]	Φ_p[c]	τ_p [μs][d]	T_{dec}/T_g [°C][e]
1	250 (4.5), 289 (5.5), 379 (1.3)	510	507	0.36	0.53	414/135
2	250 (6.3), 289 (7.5), 379 (1.7)	510	506	0.35	0.37	418/132
3	250 (4.9), 287 (6.4), 378 (1.3)	505	504	0.31	0.46	409/141
4	251 (4.8), 290 (5.5), 366 (1.3)	506	503	0.39	0.87	405/128
5	273 (8.4), 341 (1.5), 362 (1.0)	514	507	0.37	0.78	315/123
6	276 (3.9), 341 (0.8), 364 (0.5)	514	506	0.36	0.77	316/137
7	274 (5.9), 338 (1.8), 362 (0.9)	507	504	0.33	0.58	309/132
8	272 (5.3), 335 (1.1), 360 (0.7)	507	504	0.38	0.62	342/138
9	280 (5.4), 310 (3.4), 383 (0.6)	547	544	0.27	0.87	340/123

[a] Measured in CH_2Cl_2 at 298 K and extinction coefficients (10^4 M^{-1} cm^{-1}) are shown in parentheses.

[b] Measured in CH_2Cl_2 at 77 K.

[c] Measured in CH_2Cl_2 at 298 K relative to *fac*-Ir(ppy)$_3$ (Φ_p = 0.40), λ_{ex} = 400 nm.

[d] Measured in degassed toluene solutions and the excitation wavelength is set at 370 nm for all complexes.

[e] T_d is the onset decomposition temperature.

To investigate the frontier orbitals of the complexes, cyclic voltammetry (CV) was performed in degassed tetrahydrofuran solutions of the complexes containing 0.1 M tetrabutylammonium hexafluorophosphate as the supporting electrolyte at a scan rate of 100 mV s^{-1} using ferrocene as the internal standard. The results are summarized in Table 2. For the redox behavior of the Ir(III) species, it is generally accepted that the HOMO levels are mostly related to the d orbitals of iridium with some π-orbital contributions from the ligand, while the LUMO level of this kind of Ir(III) complexes is mainly attributed to the pyridyl ring of the cyclometalating ligands.[16] All of our complexes displayed reversible one-electron oxidation waves between 0.41 and 0.60 V (versus Fc/Fc^+), which can be generally assigned to the metal-centered Ir(III)/Ir(IV) oxidation couple. As seen in the data, the HOMO and LUMO energy levels could be tuned by modification of the substituents on the cyclometalating ligands. The electron-withdrawing CF_3 substituent on the pyridyl ring in **9** tends to stabilize the LUMO level, whereas the electron-donating methyl moiety shows an opposite trend in **3**–**4** and **7**–**8**.[17] Therefore, as compared to the parent complexes **1** and **5**, the attachment of the methyl group in **3**–**4** and **7**–**8** tend to decrease the electron affinities, thereby destabilizing the LUMO energy levels. On the other hand, it is observed that

the frontier orbital energy levels are relatively independent of the identity of R_1 moiety on the phenyl ring of benzyl unit. Overall, the oxidation potentials are lower for the homoleptic complexes than their corresponding heteroleptic complexes, which are in accordance with the fact that the acac ligand with the stronger ligand-field strength could stabilize the HOMO level.

Table 2 Electrochemical potentials and frontier molecular orbital energy levels of the Ir(III) complexes

Ir(III) complex	$E_{1/2}^{OX}$ [V][a]	$E_{1/2}^{RED}$ [V][a]	HOMO [eV][b]	LUMO [eV][c]	Energy gap (E_g) [eV][d]
1	0.49	–2.42	–5.29	–2.38	2.91
2	0.48	–2.43	–5.28	–2.37	2.91
3	0.41	–2.54	–5.21	–2.26	2.95
4	0.41	–2.61	–5.21	–2.19	3.02
5	0.53	–2.35	–5.33	–2.45	2.88
6	0.55	–2.37	–5.35	–2.43	2.92
7	0.42	–2.59	–5.22	–2.21	3.01
8	0.43	–2.65	–5.23	–2.15	3.08
9	0.60	–2.31	–5.40	–2.49	2.91

[a] Measured in 0.1 M $[Bu_4N]PF_6$ in THF at 298 K.

[b] Determined from HOMO = –(4.8 eV + $E_{1/2}^{OX}$).

[c] Determined from LUMO = –(4.8 eV + $E_{1/2}^{RED}$).

[d] Energy gap E_g = LUMO – HOMO.

The geometries and electronic structures of all complexes were examined by density functional theory (DFT) and time-dependent DFT (TDDFT) methods at the

B3LYP/GENECP level (see ESI). Our TDDFT calculations show that the S_0–S_1 transitions correspond to the HOMO–LUMO transitions with non-zero oscillator strengths (Table 3). The results of DFT calculations show that all the complexes have similar HOMOs and LUMOs in terms of their orbital characters (Fig. 3). The contour plots show that the HOMOs mainly consist of the d orbitals from the metal center that mix with the π orbitals of the phenyl rings that are directly bonded to the metal center. The LUMOs correspond to the lowest π orbitals of the conjugated organic ligands, in which the pyridyl rings contribute more. In general, electronic effects have been considered owing to their profound influence on the orbital energies as well as the relative ease with which the electron-withdrawing (i.e. -CF_3) and electron-donating (e.g. methyl) groups can be incorporated into the ligand structure. Electron-withdrawing substituents on pyridine tend to stabilize the HOMO by removing electron density from the metal, whereas the electron-donating moieties have an inverse effect. On the other hand, the S_0–T_1 energy gap at the optimized geometries can be obtained from the computational studies.

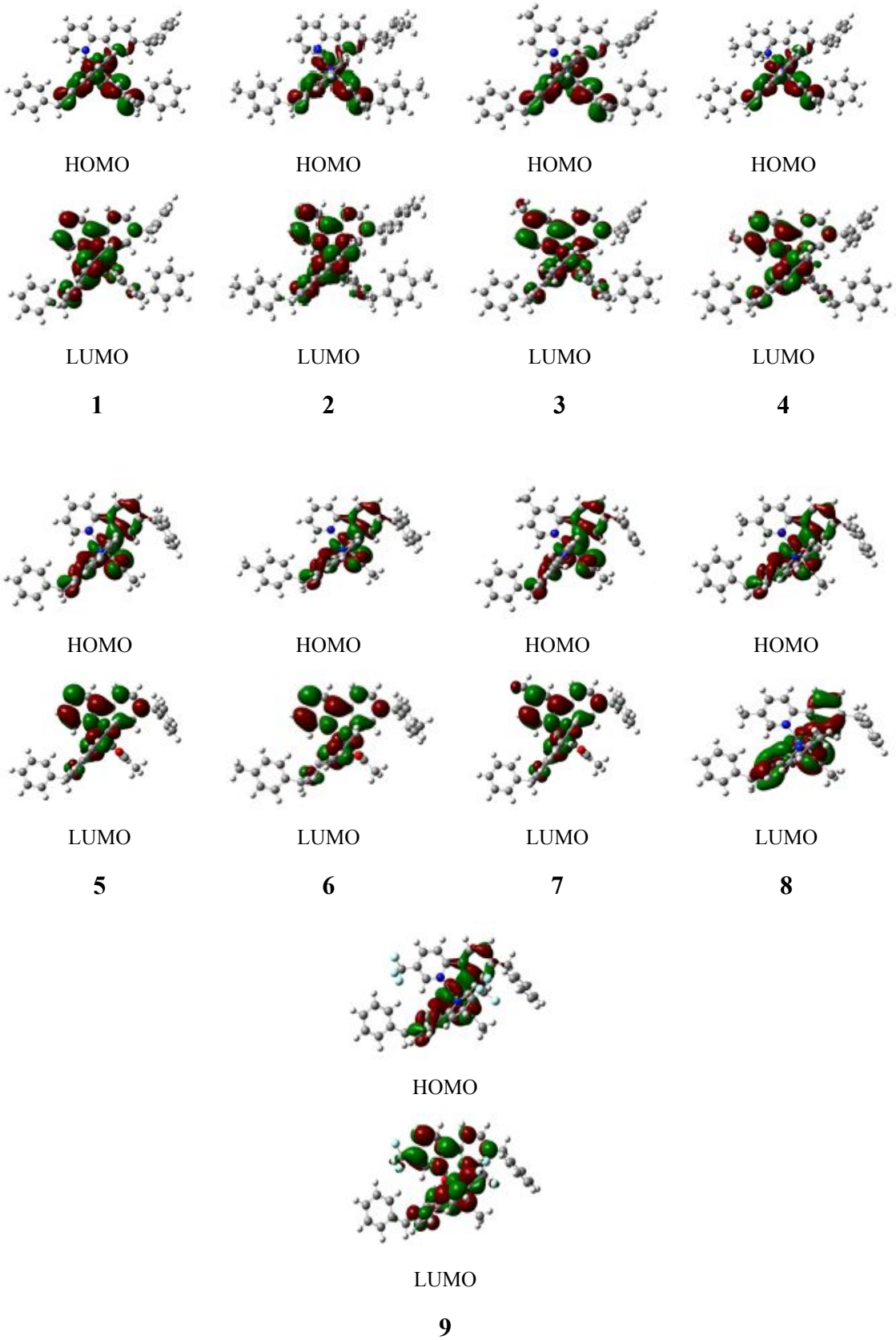

Fig. 3 Electron density maps on the HOMO and LUMO of the complexes **1–9**.

Table 3 Computational data of Ir(III) complexes

Complex	The oscillator strength (*f*) of the $S_0 \rightarrow S_1$ transition	The largest coefficient in the Cl expansion of the S_1 state[a] ($S_0 \rightarrow S_1$ excitation energy)
1	0.0222	H→L: 0.63235 (449 nm)
2	0.0224	H→L: 0.62347 (449 nm)
3	0.0268	H→L: 0.66255 (438 nm)
4	0.0213	H→L: 0.59737 (449 nm)
5	0.0076	H→L: 0.68331 (430 nm)
6	0.0072	H→L: 0.68400 (429 nm)
7	0.0088	H→L: 0.68068 (427 nm)
8	0.0079	H→L: 0.68835 (431 nm)
9	0.0066	H→L: 0.70106 (471 nm)

[a] Cl stands for configuration interaction. H→L represent the HOMO to LUMO transition. Only the main configurations are presented.

A good combination of the attractive Φ_p and high thermal stabilities, good film-forming properties and short τ_p renders this kind of Ir(III) complex advantageous for efficient optoelectronic devices. To evaluate their EL performance, a series of OLED devices **D1** to **D9** have been fabricated with a simple configuration of ITO/MoO_3 (10 nm)/NPB (70 nm)/TCTA (5 nm)/TCTA:dopant (8 wt.-%, 20 nm)/TPBi (35 nm)/LiF (1 nm) /Al (ITO: indium tin oxide; MoO_3: molybdenum trioxide; NPB: *N*,*N*'-diphenyl-*N*,*N*'-bis(1-naphthyl)-(1,18-biphenyl)-4,4-diamine;

TCTA: 4,4',4''-tri(*N*-carbazolyl)triphenylamine; TPBi: tris(*N*-phenylbenzimidizol-2-yl)benzene ; LiF: lithium fluoride; Al: aluminum). The structure of multilayer OLEDs and the molecular structures of compounds involved in their fabrication are depicted in Fig. 4. OLEDs were fabricated by thermal vacuum deposition approach of layered materials onto the surface of an ITO-coated glass substrate. MoO_3 was then coated on the pre-cleaned ITO surface as hole-injecting layer (HIL). It is noted that MoO_3 can reasonably match the work function of ITO in order to reduce the hole-injection barrier of the device.[18] TCTA and NPB act as hole-transporting layer (HTL) concurrently. The low HOMO and high LUMO levels of TCTA can alleviate the difficulty for the injection of hole to the phosphor.[19] Therefore, TCTA also serves as a small-molecular host material for all these phosphorescent emitters. Films of Ir(III) complexes doped in TCTA were adopted as the emitting layer (EML). TPBi was introduced as electron-transporting/hole-blocking layer (ETL/HBL) due to its excellent hole blocking ability and good electron mobility.[20] LiF acts as an electron-injection layer.

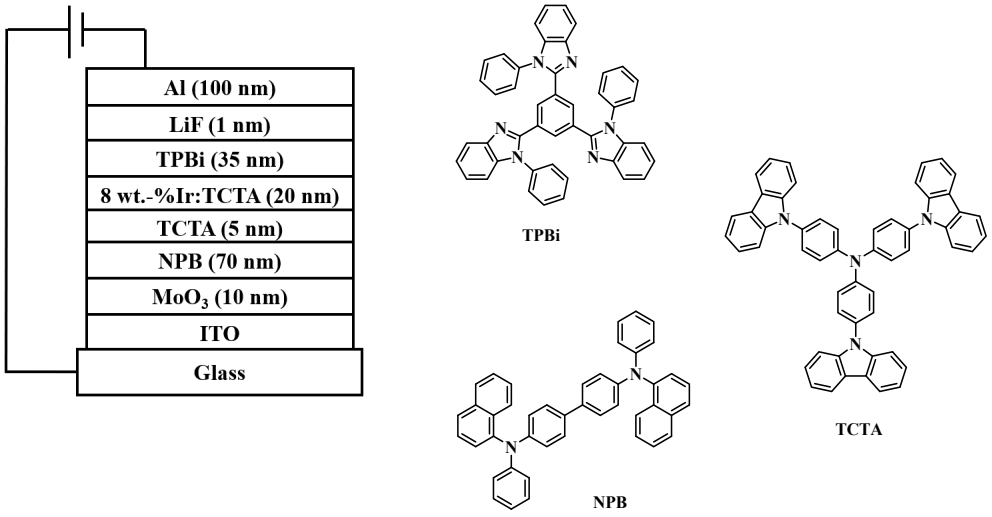

Fig. 4 General device configuration and the molecular structures of the key compounds used in the device.

Each of the devices exhibits a strong voltage-independent EL signal with no guest-concentration dependence, which is only slightly red-shifted from the corresponding PL spectrum observed in the solution state (Fig. S10 in ESI). The close resemblance between their PL and EL spectra indicates the absence of aggregation or π-π stacking, which represents the merit of this new molecular design strategy by using benzyl group in the phosphors. The origin of EL emission from the triplet excited states of Ir(III) cyclometallates was confirmed. The energy transfer from the host exciton to the iridophosphors occurs efficiently upon electrical excitation as no emission from other layers was observed in each device even at high current densities.[21] Devices **D1**–**D8** present intense bluish-green or green emissions with the EL maximum at 508–520 nm (Fig. 5). From Table 4 that summarizes all the device performance parameters, it can be clearly observed that device **D4** with 8 wt.-%

doping level achieved the best EL performance of more than 51.1 lm W^{-1} for power efficiency (η_P) and 21.4% for external quantum efficiency (η_{ext}). It exhibited a maximum brightness (L_{max}) of 48354 cd m^{-2}. By adding the benzyl group to the ppy ligand in benchmark complexes *fac*-Ir(ppy)$_3$ and Ir(ppy)$_2$(acac), devices **D1** and **D5** outperformed those fabricated with *fac*-Ir(ppy)$_3$ and Ir(ppy)$_2$(acac) under the same device structure and conditions (Table 4 and Fig. 6). As compared with its isomer (**3** in device **D3**), the optimized device performance of **3** was achieved with lower values of η_P, η_{ext} and luminance efficiency (η_L) of 33.0 lm W^{-1}, 16.2% and 55.7 cd A^{-1}, respectively. On the other hand, the performance of the heteroleptic congener **8** is also impressive. Device **D8** displayed the luminance of 48127 cd m^{-2}, η_{ext} of 19.1%, η_L of 70.1 cd A^{-1} and η_P of 23.9 lm W^{-1}, which outperformed those of the [Ir(ppy)$_2$(acac)]-doped device (Table 4). Therefore, improved EL performance can be readily achieved by modifying the ppy ligand with the conjugation-breaking benzyl group, which can tune the properties of Ir(III) complexes (Fig. 7). Consistent with the literature data,[22] compounds **4** and **8** with methyl group at the 5-position of the pyridyl ring showed better performance than compounds **1** and **5**, respectively, since the methyl group can decrease the self-quenching effect while increasing their compatibility with the organic host material to improve the EL performance of the device. Hence, both the effects of methyl substituent at the 5-position of pyridine and

benzyl group can enhance the performance of devices **D4** and **D8**. By changing the substituent on the organic chromophore, device **D9** fabricated from complex **9** showed an orange-yellow emission at 548 nm. A maximum brightness of 28402 cd m^{-2} was achieved with the η_L, η_{ext}, and η_P of 10.22 cd A^{-1}, 23.27% and 37.9 lm W^{-1}, respectively. Since device **D9** emits at a much longer wavelength than other devices **D5**–**D8**, there is a notable drop in the efficiency values generally, in accordance with the energy gap law. All of the devices show low turn-on voltage (V_{on}) of no more than 3.1 V, which indicate that a balanced charge transportation occur in all the devices. In addition, the efficiency roll-off at high current densities is not severe in most of our devices, implying that the triplet-triplet annihilation effect is not very significant at high current densities (Fig. 7). All these exciting results can be attributed to the effect induced by the benzyl group.

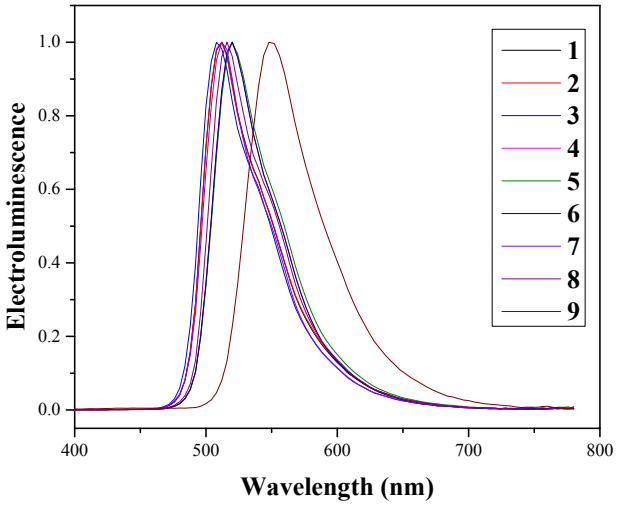

Fig. 5 EL spectra of **1**–**9**.

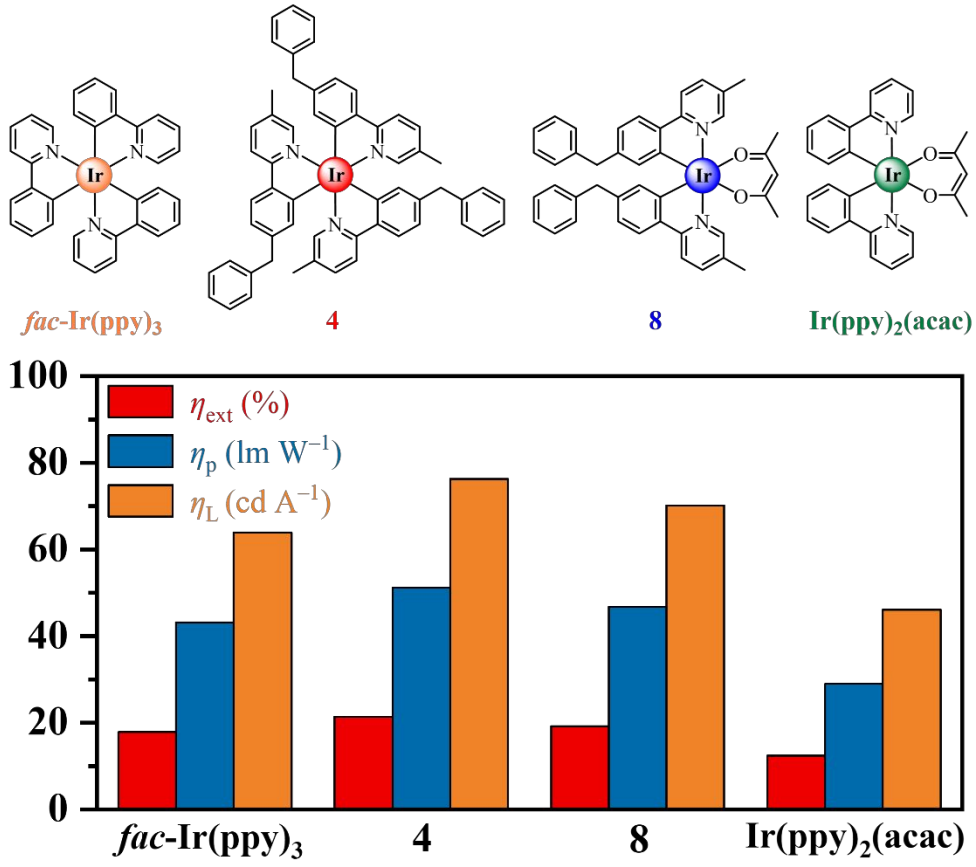

Fig. 6 Comparison of the device performance of **4** and **8** versus benchmark materials.

Table 4 Performance parameters of the electrophosphorescent OLEDs

OLED	Phosphor dopant (8 wt.-%)	V_{on} [V]	L_{max} [cd m^{-2}][a]	η_{ext} [%][a]	η_p [lm W^{-1}][a]	η_L [cd A^{-1}][a]	λ_{max} [nm][b]
D1	**1**	2.9	48344	12.43	26.26	43.5	512 (0.26, 0.63)
D2	**2**	3.1	48443	11.49	23.83	40.9	512 (0.28, 0.63)
D3	**3**	3.1	48477	16.20	33.00	55.7	508 (0.25, 0.64)

D4	**4**	2.9	48354	21.39 (12.41)	51.12 (13.49)	76.3 (44.26)	512 (0.27, 0.64)
D5	**5**	2.9	48319	16.50	39.55	61.7	520 (0.29, 0.65)
D6	**6**	2.7	48341	16.17	37.78	60.8	520 (0.29, 0.65)
D7	**7**	2.9	17830	16.24	39.24	57.3	512 (0.26, 0.64)
D8	**8**	2.7	48127	19.14 (10.31)	46.70 (12.14)	70.1 (37.82)	516 (0.28, 0.65)
D9	**9**	3.1	28402	10.22	23.27	37.9	548 (0.42, 0.56)
S1	*fac*-Ir(ppy)$_3$	2.9	48516	17.85	43.17	63.9	516 (0.29, 0.64)
S2	Ir(ppy)$_2$(acac)	2.9	48235	12.42	28.99	46.1	520 (0.28, 0.65)

[a] Maximum values of the devices. Values in parenthesis refer to those measured at 100 mA cm^{-2}.

[b] Values were collected at 8 V and CIE coordinates (x,y) are shown in parentheses.

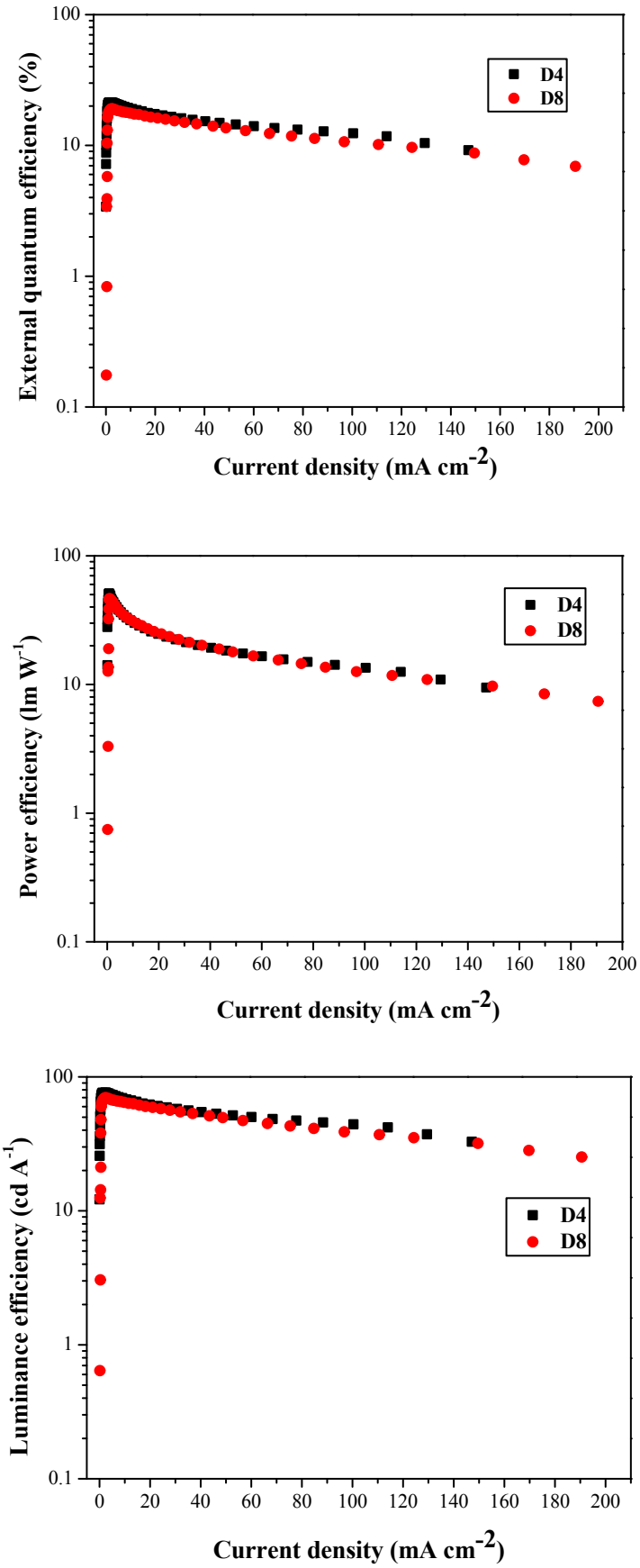

Fig. 7 Relationship between EL efficiencies and current density for the devices **D4**

and **D8**.

Conclusions

Herein, a series of phosphorescent cyclometalated Ir(III) complexes containing bppy ligand have been synthesized and characterized. We have extensively investigated the effect of the position of methyl substituents and the nature of substituents on the photophysics, electrochemistry, and electrophosphorescent properties of the materials. The performance of these emitters in device applications depends heavily on the ligand substituent effects and their excited-state properties. The good morphological stability and short triplet excited state lifetimes together with the high phosphorescence yield of these complexes would favor the realization of highly efficient OLED devices. The OLED performances for these phosphors have also been investigated. Device **D4** containing metallophosphor **4** showed the best performance with η_L of 76.3 cd A^{-1}, η_P of 51.1 lm W^{-1}, η_{ext} of 21.4% and exhibited the L_{max} of 48354 cd m^{-2}. These molecules show superior performance to that of the state-of-the-art phosphor with the neat ppy group in the same device structure and fabrication condition. Given the ease of synthesis and color tunability as well as performance advantages, the present demonstration has a significant potential for applications in multicolor displays and possibly in light illumination sources with

other suitable emissive dopants by emission layer combination.

Experimental

Synthesis of complexes 1–9

General procedures for the synthesis of homoleptic cyclometalated iridium(III) complexes: According to the literature report, the homoleptic cyclometalated Ir(III) complexes were synthesized by a one-pot reaction. A mixture of cyclometalating ligand and [$Ir(acac)_3$] was dissolved in glycerol and heated at 220 ^oC for 24 h under nitrogen. After cooling, the reaction mixture was diluted with D.I. water and extracted with CH_2Cl_2. Subsequently, the organic layer was dried over Na_2SO_4 and concentrated under reduced pressure. The complex was purified by column chromatography over silica gel eluting with a mixture of CH_2Cl_2/hexane.

1: Yellow powder (37.4%).

Spectral data: MS (MALDI-TOF): *m/z* 925.30 (M^+). ^1H NMR ($CDCl_3$): δ (ppm) 7.80 (d, *J* = 8.0 Hz, 3H, Ar), 7.57–7.53 (m, 6H, Ar), 7.50 (d, *J* = 5.6 Hz, 3H, Ar), 7.10–7.02 (m, 15H, Ar), 6.83 (s, 6H, Ar), 6.63 (d, *J* = 8.4 Hz, 3H, Ar), 3.73–3.70 (m, 6H, CH_2). ^{13}C NMR ($CDCl_3$): δ (ppm) 166.62, 161.65, 146.76, 142.26, 141.43, 139.21, 138.08, 135.64, 134.67, 128.76, 128.46, 124.06, 121.34, 120.41, 116.40 (Ar),

41.76 (CH_2).

2: Yellow powder (33.9%).

Spectral data: MS (MALDI-TOF): *m/z* 967.41 (M^+). ^{1}H NMR ($CDCl_3$): δ (ppm) 7.80 (d, *J* = 8.0 Hz , 3H, Ar), 7.54–7.51 (m, 9H, Ar), 6.97 (d, *J* = 8.0 Hz, 6H, Ar), 6.86–6.81 (m, 12H, Ar), 6.64 (d, *J* = 9.6 Hz, 3H, Ar), 3.65 (d, *J* = 6.0 Hz, 6H, CH_2), 2.17 (s, 9H, CH_3). ^{13}C NMR ($CDCl_3$): δ (ppm) 166.77, 161.80, 146.99, 142.49, 141.65, 139.31, 138.16, 135.74, 134.76, 128.85, 128.55, 124.12, 121.48, 120.61, 116.47 (Ar), 41.82 (CH_2), 20.93 (CH_3).

3: Yellow powder (32.3%).

Spectral data: MS (MALDI-TOF): *m/z* 967.32 (M^+). ^{1}H NMR ($CDCl_3$): δ (ppm) 7.59 (s, 3H, Ar), 7.51 (d, *J* = 10.4 Hz, 3H, Ar), 7.36 (d, *J* = 5.2 Hz, 3H, Ar), 7.11–7.00 (m, 15H, Ar), 6.84 (s, 3H, Ar), 6.65 (d, *J* = 6.0 Hz, 3H, Ar), 6.60 (d, *J* = 7.6 Hz, 3H, Ar), 3.68 (d, *J* = 6.0 Hz, 6H, Ar), 2.38 (s, 9H, CH_3). ^{13}C NMR ($CDCl_3$): δ (ppm) 166.26, 162.17, 146.82, 146.51, 142.51, 138.18, 128.73, 128.10, 125.44, 123.77, 122.69, 120.52, 119.11 (Ar), 42.35 (CH_2), 21.35 (CH_3).

4: Yellow powder (40.6%).

Spectral data: MS (MALDI-TOF): *m/z* 967.36 (M^+). ^{1}H NMR ($CDCl_3$): δ (ppm) 7.70 (d, *J* = 8.4 Hz, 3H, Ar), 7.50 (d, *J* = 8.0 Hz, 3H, Ar), 7.37 (d, *J* = 10.4 Hz, 3H, Ar), 7.28 (s, 3H, Ar), 7.11–7.00 (m, 15H, Ar), 6.80 (s, 3H, Ar), 6.61 (d, *J* = 7.6 Hz, 3H, Ar), 3.69 (d, *J* = 5.2 Hz, 6H, CH_2), 2.12 (s, 9H, CH_3). ^{13}C NMR ($CDCl_3$): δ (ppm) 164.00, 146.87, 142.46, 141.59, 138.09, 136.73, 130.92, 128.70, 128.09, 125.42, 123.45, 118.02 (Ar), 42.33 (CH_2), 18.38 (CH_3).

General procedures for the synthesis of heteroleptic cyclometalated iridium(III) complexes: Heteroleptic cyclometalated Ir(III) complexes were prepared via two reaction steps. 2.5 Equivalents of the corresponding cyclometalating ligand reacted with $IrCl_3{\cdot}nH_2O$ in a mixture of 2-ethoxyethanol:H_2O (3:1, v/v). The mixture was stirred at 80 ^{o}C overnight to yield the chloro-bridged dimer. Precipitates were formed gradually. The crude Ir(III) dimer was dried and used for the subsequent reaction without further purification. Acetylacetone and sodium carbonate were mixed with Ir(III) dimer in 2-ethoxyethanol solution. The reaction mixture was refluxed for 16 h under nitrogen and then cooled to room temperature. The mixture was washed with D.I. water and extracted with CH_2Cl_2. The organic layer was dried over Na_2SO_4 and concentrated under reduced pressure. The complex was purified by column chromatography over silica gel using a mixture of CH_2Cl_2/hexane.

5 : Yellow powder (28.1%).

Spectral data: MS (MALDI-TOF): *m/z* 779.95 (M^+). ^{1}H NMR ($CDCl_3$): δ (ppm) 8.43 (d, *J* = 6.4 Hz, 2H, Ar), 7.73 (d, *J* = 7.6 Hz, 2H, Ar), 7.67–7.63 (m, 2H, Ar), 7.41 (d, *J* = 8.0 Hz, 2H, Ar), 7.17–7.10 (m, 6H, Ar), 7.07–7.03 (m, 2H, Ar), 6.95 (d, *J* = 8.0 Hz, 2H, Ar), 6.55 (d, *J* = 9.6 Hz, 2H, Ar), 6.02 (s, 2H, Ar), 5.21 (s, 1H, acac), 3.68 (s, 4H, CH_2), 1.78 (s, 6H, CH_3). ^{13}C NMR ($CDCl_3$): δ (ppm) 184.50 (CO), 168.45, 148.06, 147.57, 142.70, 141.43, 141.24, 136.63, 133.72, 129.03, 128.08, 125.53, 123.75, 121.41, 120.93, 118.10 (Ar), 100.39 (CH), 41.79 (CH_2), 28.80 (CH_3).

6 : Yellow powder (26.8%).

Spectral data: MS (MALDI-TOF): *m/z* 808.32 (M^+). ^{1}H NMR ($CDCl_3$): δ (ppm) 8.42 (d, *J* = 6.4 Hz, 2H, Ar), 7.35 (d, *J* = 8.0 Hz, 2H, Ar), 7.67–7.63 (m, 3H, Ar), 7.40 (d, *J* = 8.0 Hz, 2H, Ar), 7.06–7.03 (m, 2H, Ar), 6.96 (d, *J* = 8.0 Hz, Ar, 4H), 6.85 (d, *J* = 8.0 Hz, Ar, 4H), 6.54 (d, *J* = 9.6 Hz, 2H, Ar), 6.01 (s, 2H, Ar), 5.20 (s, 1H, acac), 3.64 (s, 4H, CH_2), 2.18 (s, 6H, CH_3), 1.78 (s, 6H, CH_3). ^{13}C NMR ($CDCl_3$): δ (ppm) 184.51 (CO), 168.50, 148.08, 147.54, 142.63, 141.74, 138.13, 136.56, 134.87, 133.69, 128.93, 128.79, 123.73, 121.35, 120.88, 118.06 (Ar), 41.32 (CH_2), 28.75 (CH_3), 21.02 (CH_3).

7 : Yellow powder (25.3%).

Spectral data: MS (MALDI-TOF): *m/z* 808.1 (M^+). ^{1}H NMR ($CDCl_3$): δ (ppm) 8.23 (d, *J* = 5.6 Hz, 2H, Ar), 7.52 (s, 2H, Ar), 7.38 (d, *J* = 8.0 Hz, 2H, Ar), 7.16–7.10 (m, 6H, Ar), 6.95 (d, *J* = 8.0 Hz, 4H, Ar), 6.86 (d, *J* = 7.2 Hz, 2H, Ar), 6.54 (d, *J* = 9.6 Hz, 2H, Ar), 6.02 (s, 2H, Ar), 5.18 (s, 1H, acac), 3.69 (s, 4H, CH_2), 1.76 (s, 6H, CH_3). ^{13}C NMR ($CDCl_3$): δ (ppm) 184.37 (CO), 172.36, 167.81, 147.45, 142.87, 141.13, 133.85, 129.11, 128.03, 125.44, 123.46, 122.13, 121.27, 118.85 (Ar) 41.72 (CH_2), 28.76 (CH_3), 21.42 (CH_3).

8 : Yellow powder (32.7%).

Spectral data: MS (MALDI-TOF): *m/z* 808.12 (M^+). ^{1}H NMR ($CDCl_3$): δ (ppm) 8.22 (s, 2H, Ar), 7.61 (d, *J* = 8.4 Hz, 2H, Ar), 7.45 (d, *J* = 10.0 Hz, 2H, Ar), 7.36 (d, *J* = 8.0 Hz, 2H, Ar), 7.17–7.11 (m, 6H, Ar), 6.97 (d, *J* = 8.0 Hz, 4H, Ar), 6.55 (d, *J* = 9.6 Hz, 2H, Ar), 5.97 (s, 2H, Ar), 5.21 (s, 1H, Ar), 3.70 (s, 4H, CH_2), 2.35 (s, 6H, CH_3), 1.80 (s, 6H, CH_3). ^{13}C NMR ($CDCl_3$): δ (ppm) 184.40 (CO), 165.70, 147.76, 146.69, 142.99, 141.24, 140.85, 137.54, 133.53, 130.62, 129.13, 128.05, 125.52, 123.19, 121.28, 117.68 (Ar), 100.47 (CH), 41.74 (CH_2), 28.85 (CH_3), 18.52 (CH_3).

9 : Orange powder (25.6%).

Spectral data: MS (MALDI-TOF): *m/z* 915.94 (M^+) ^{1}H NMR ($CDCl_3$): δ (ppm) 8.62 (s, 2H, Ar), 7.79 (d, *J* = 5.6 Hz, 4H, Ar), 7.44 (d, *J* = 7.2 Hz, 2H, Ar), 7.24 (s, 6H, Ar), 6.93 (s, 4H, Ar), 6.63 (d, *J* = 7.2 Hz, 2H, Ar), 5.89 (s, 2H, Ar), 5.23 (s, 1H, acac), 3.70 (s, 4H, CH_2), 1.79 (s, 6H, CH_3). ^{13}C NMR ($CDCl_3$): δ (ppm) 184.29 (CO), 148.39, 144.10, 142.43, 139.32, 132.99, 132.45, 128.07, 127.13, 124.76, 124.26, 123.47, 122.39, 121.01, 116.74, 115.69 (Ar) 99.86 (CH), 40.68 (CH_2), 28.68 (CH_3), 13.11 (CF_3).

Conflicts of interest

There are no conflicts to declare.

Acknowledgements

This work was supported by the National Key R&D Program of China (2022YFE0104100), National Natural Science Foundation of China (52073242), ITC Guangdong-Hong Kong Technology Cooperation Funding Scheme (TCFS) (GHP/038/19GD), CAS-Croucher Funding Scheme for Joint Laboratories (ZH4A), the Hong Kong Research Grants Council (PolyU 15301922), Miss Clarea Au for the Endowed Professorship in Energy (847S) and Research Institute for Smart Energy (CDAQ).

References

1. (*a*) J. H. Burroughes, D. D. C. Bradley, A. R. Brown, R. N. Marks, K. Mackay, R. H. Friend, P. L. Burns and A. B. Holmes, *Nature*, 1990, **347**, 539; (*b*) C. H. Chen, J. Shi and C. W. Tang, *Macromol. Symp*., 1997, **125**, 1; (*c*) M. A. Baldo, D. F. O'Brien, Y. You, A. Shoustikov, S. Sibley, M. E. Thompson and S. R. Forrest, *Nature*, 1998, **395**, 151; (*d*) N. Matsusue, Y. Suzuki and H. Naito, *Jpn. J. Appl. Phys.*, 2005, **44**, 3691; (*e*) G. J. Zhou, W.-Y. Wong, B. Yao, Z. Xie and L. Wang, *J. Mater. Chem.*, 2008, **18**, 1799; (*f*) J.-H. Jou, C.-Y. Hsieh, J.-R. Tseng, S.-H. Peng, Y.-C. Jou, J. H. Hong, S.-M. Shen, M.-C. Tang, P.-C. Chen and C.-H. Lin, *Adv. Funct. Mater.*, 2013, **23**, 2750.

2. (*a*) C. Adachi, M. A. Baldo, M. E. Thompson and S. R. Forrest, *J. Appl. Phys.*, 2001, **90**, 5048; (*b*) C.-H. Yang, Y.-M. Cheng, Y. Chi, C.-J. Hsu, F.-C. Fang, K.-T. Wong, P.-T. Chou, C.-H. Chang, M.-H. Tsai and C.-C. Wu, *Angew. Chem. Int. Ed.*, 2007, **46**, 2418.

3. (*a*) S. Bettington, M. Tavasli, M. R. Bryce, A. Beeby, H. Al-Attar and A. P. Monkman, *Chem. Eur. J.*, 2007, **13**, 1423; (*b*) B.-S. Du, J.-L. Liao, M.-H. Huang, C.-H. Lin, H.-W. Lin, Y. Chi, H.-A. Pan, G.-L. Fan, K.-T. Wong, G.-H. Lee and P.-T. Chou, *Adv. Funct. Mater.*, 2012, **22**, 3491; (*c*) Y. You and S. Y. Park, *Dalton Trans*., 2009, 1267; (d) W.-Y. Wong and S.-Y. Poon, *J. Inorg. Organomet. Polym.* 2008, **18**, 155.

4. (*a*) Y. Y. Lyu, Y. Byun, O. Kwon, E. Han, W. S. Jeon, R. R. Das and K. Char, *J. Phys. Chem. B.*, 2006, **110**, 10303; (*b*) G. Zhou, Q. Wang, C.-L. Ho, W.-Y. Wong, D. Ma, L. Wang and Z. Lin, *Chem. Asian J.*, 2008, **3**, 1830; (*c*) W.-Y. Wong and C.-L. Ho, *Coord. Chem. Rev.*, 2009, **253**, 1709; (*d*) J. Li, P. I. Djurovich, B. D. Alleyne, M. Yousufuddin, N. N. Ho, J. C. Thomas, J. C. Peters, R. Bau and M. E.

Thompson, *Inorg. Chem.*, 2005, **44**, 1713.

5. (*a*) K. Dedeian, J. Shi, N. Shepherd, E. Forsythe and D. C. Morton, *Inorg. Chem*., 2005, **44**, 4445; (*b*) A. Beeby, S. Bettington, I. D. W. Samuel and W. Z. Wang, *J. Mater. Chem*., 2003, **13**, 80; (*c*) G. Zhou, W.-Y. Wong and X. Yang, *Chem. Asian. J.*, 2011, **6**, 1706.
6. G. Zhou, C.-L. Ho, W.-Y. Wong, Q. Wang, D. Ma, L. Wang, Z. Lin, T. B. Marder and A. Beeby, *Adv. Funct. Mater.*, 2008, **18**, 499.
7. C. Liu, X. Rao, X. Lv, J. Qiu and Z. Jin, *Dyes Pigm.*, 2014, **109**, 13.
8. S. Langle, M. Abarbri, A. Duchêne, *Tetrahedron Lett.*, 2003, **44**, 9255.
9. J. H. Seo, I. J. Kim, Y. K. Kim and Y. S. Kim, *Jpn. J. Appl. Phys.*, 2008, **48**, 6987.
10. P. J. Spellane and R. J. Watts, *Inorg. Chem.,* 1993, **32**, 5633.
11. C.-L. Ho, W.-Y. Wong, G. J. Zhou, B. Yao, Y. Xie and L. X. Wang, *Adv. Funct. Mater.*, 2007, **17**, 2925.
12. W.-Y. Wong and C.-L. Ho, *Coord. Chem. Rev.*, 2009, **253**, 1709.
13. M. Mydlak, C. Bizzarri, D. Hartmann, W. Sarfert, G. Schmid and L. De Cola, *Adv. Funct. Mater.,* 2010, **20**, 1812.
14. M. A. Baldo, S. Lamansky, P. E. Burrows, M. E. Thompson and S. R. Forrest, *Appl. Phys. Lett.*, 1999, **75**, 4.
15. Y. Wang, N. Herron, V. V. Grushin, D. LeClouxa and V. Petrov, *Appl. Phys. Lett*., 2001, **79**, 449–451.
16. V. V. Grudhin, N. Herron, D. D. LeCloux, W. J. Marshell, V. A. Petrov and Y. Wang, *Chem Commun.*, 2001, 1494.
17. X. R. Zhang, R. Kostecki, T. J. Richardson, J. K. Pugh and P. N. Ross, *J.*

Electrochem. Soc., 2001, **148**, A1341.

18. H. Jang, C. H. Shin, N. G. Kim, K. Y. Hwang and Y. Do, *Synth. Met*., 2005, **154**, 157.

19. D.-H. Lee, Y.-P. Liu, K.-H. Lee, H. Y. Chae and S. M. Cho, *Org. Electron.*, 2010, **11**, 427.

20. B. Liu, M. Xu, L. Wang, H. Tao, Y. Su, D. Gao, J. Zou, L. Lan and J. Peng, *ECS J. Solid State Sci. Technol.*, 2013, **2**, R258.

21. V. K. Rai, M. Nishiura, M. Takimoto and Z. Hou, *Chem Commun.*, 2011, **47**, 5726.

22. G. Tan, S. Chen, N. Sun, Y. Li, D. Fortin, W.-Y. Wong, H.-S. Kwok, D. Ma, H. Wu, L. Wang and P. D. Harvey, *J. Mater. Chem. C.*, 2013, **1**, 808.

Electronic Supporting Information

Highly efficient iridium(III) phosphors with 2-(4-benzylphenyl)pyridine-type ligand and their high-performance organic light-emitting diodes

Wai-Yeung Wong,*[abcd] Nga-Yuen Chau,[d] Qiwei Wang,[ad] Lu Jiang,[a] Junlong Li[a] and Dongge Ma*[e]

[a] *Antibiotics Research and Reevaluation Key Laboratory of Sichuan Province, Sichuan Industrial Institute of Antibiotics, Chengdu University, Chengdu 610052, P. R. China*

[b] *Department of Applied Biology and Chemical Technology, The Hong Kong Polytechnic University, Hung Hom, Hong Kong, P. R. China. E-mail: wai-yeung.wong@polyu.edu.hk*

[c] *The Hong Kong Polytechnic University Shenzhen Research Institute, Shenzhen 518057, P. R. China*

[d] *Department of Chemistry and Institute of Advanced Materials, Hong Kong Baptist University, Waterloo Road, Kowloon Tong, Hong Kong, P. R. China*

[e] *State Key Laboratory of Luminescent Materials and Devices, Center for Aggregation-Induced Emission, South China University of Technology, Guangzhou 510640, P. R. China. E-mail: msdgma@scut.edu.cn*

Experimental section

General procedures and materials: All reactions were performed under an inert nitrogen atmosphere with the use of a Schlenk line. Glasswares were dried in oven prior to use. Commercially available reagents were used without purification unless otherwise stated. Solvents were purified by distillation over appropriate drying agents. All reactions were monitored by thin-layer chromatography (TLC) with Merck pre-coated aluminum plates. Products were separated and purified by column chromatography with silica gel. Compounds $Ir(acac)_3$, $IrCl_3.3H_2O$, K_2PtCl_4, $Pd(PPh_3)_4$, 4-bromobenzylbromide and other starting materials were commercially available and used as received unless otherwise specifically mentioned. The aryl boronic acid was prepared as reported by the literature method.[1]

Physical measurements: Fast atom bombardment (FAB) mass spectra were recorded on a Finnigan MAT SSQ710 system. Proton and carbon NMR spectra were measured in $CDCl_3$ on a Bruker Ultra-shield 400 MHz spectrometer and tetramethylsilane (TMS) was used as an internal standard for chemical shift calibration. UV/Vis spectra were recorded on a Hewlett Packard 8453 spectrometer. The photoluminescent properties of the compounds were examined using PTI Time Master Model C-720 spectrometer. The photoluminescence quantum yields were investigated in degassed CH_2Cl_2 solution at 298 K against *fac*-[$Ir(ppy)_3$] standard (Φ_p = 0.40). For lifetime measurements, the 337 nm line of a N_2 laser was used as an excitation light source. The data were analyzed by iterative convolution of the luminescence decay profile with the instrument response function using a software package provided by PTI instruments. Electrochemical measurements were conducted

on Potentiostat/Galvanostat/EIS Analyzer model Parstat 4000 at a scan rate of 50 mV s^{-1}. A conventional compartment cell equipped with a carbon glassy working electrode, platinum wire counter electrode and Ag/Ag^{+} reference electrode was used. 0.1 M $[Bu_4N]PF_6$ in THF solution and ferrocene were used as a supporting electrolyte and an internal standard, respectively. The HOMO and LUMO energy levels were determined from the oxidation (E_{ox}) and reduction (E_{red}) potentials using the equations $E_{HOMO} = -(Eox + 4.8)$ eV and $E_{LUMO} = -(E_{red} + 4.8)$ eV which were calculated using the internal standard ferrocene value of -4.8 eV with respect to the vacuum level.[2] Differential scanning calorimetry (DSC) was performed on a Perkin Elmer Pyris Diamond DSC unit under a nitrogen flow at a heating rate of 20 ^{o}C min^{-1} to obtain the glass transition temperature (T_g). The thermal gravimetric analysis (TGA) was conducted on Perkin Elmer TG-6 instrument under nitrogen at the heating rate of 5 ^{o}C min^{-1}.

General procedures for OLED fabrication and measurements: The devices were fabricated by sequentially depositing organic layers under high vacuum thermal evaporation on pre-cleaned indium tin oxide (ITO) glass substrates which were treated with ozone for 10 min. For monochromatic OLEDs manufactured by vacuum deposition, the NPB layer was deposited on a 10 nm MoO_3 thin layer pre-coated on the ITO glass. Then the TCTA layer was placed on the NPB layer. The metallophosphor dopant and host material were co-evaporated to form the emitting layer. TPBi, LiF and Al were evaporated and deposited one by one. All experiments and measurements were performed at room temperature under ambient conditions. The EL spectra and luminance were measured with a PR 650 Spectra Scan spectrometer. The current density-voltage (*L-V*) characteristics of the devices were

recorded using a Keithley 2400/2000 source meter.

Synthesis of cyclometalating ligands L1–L5

Synthesis of L1

The commercially available 4-bromobenzyl bromide (1.12 g, 4.52 mmol) reacted with one equivalent of phenylboronic acid (0.55 g, 4.52 mmol) in the presence of $Pd(PPh_3)_4$ (80 mg) in the solution of toluene (40 mL), ethanol (20 mL) and 2 M Na_2CO_3 (3 mL). A two-necked flask containing 4-benzylphenyl bromide (0.80 g, 3.62 mmol) in dry tetrahydrofuran was cooled in an ice-acetone bath under a nitrogen atmosphere. Then *n*-butyllithium was added to the flask dropwisely followed by trimethylborate and diluted hydrochloric acid. 4-Benzylphenyl boronic acid (0.54 g, 2.53 mmol) was prepared, treated with 2-bromopyridine (0.31 g, 1.95 mmol) through the Suzuki coupling reaction to yield the target compound. The reaction mixture was extracted with ethyl acetate and washed with deionized (D.I.) water. The organic layer was dried over anhydrous Na_2SO_4. The solvent was filtered and then concentrated under vacuum. The mixture was purified by a silica gel column chromatography to afford the white solid product (67%).

Spectral data: MS (MALDI-TOF): *m/z* 245.12 (M^+). ^1H NMR ($CDCl_3$): δ (ppm) 7.80 (d, *J* = 8.0 Hz, 3H, Ar), 7.57–7.53 (m, 6H, Ar), 7.50 (d, *J* = 5.6 Hz, 3H, Ar), 7.10–7.02 (m, 15H, Ar), 6.83 (s, 6H, Ar), 6.63 (d, *J* = 8.4 Hz, 3H, Ar), 3.73–3.70 (m, 6H, CH_2).

Synthesis of L2

A reaction flask was charged with ethanol (20 mL), toluene (40 mL), 4-bromobenzyl bromide (1.18 g, 4.78 mmol) and *p*-tolylboronic acid (0.65 g, 4.78

mmol). The flask was evacuated and filled with nitrogen and then 2 M solution of Na_2CO_3 (3 mL) and $Pd(PPh_3)_4$ (80 mg) were added. The reaction mixture was stirred at 80 ^oC for 15 h. 1-Bromo-4-(4-methylbenzyl)benzene was then purified and then converted to its boronic acid derivative. A mixture of 4-(4-methylbenzyl)phenylboronic acid (0.61 g, 2.68 mmol) and 2-bromopyridine (0.32 g, 2.06 mmol) and tetrahydrofuran was charged with nitrogen, after which a catalytic amount of $Pd(PPh_3)_4$ was added. The mixture was stirred for two days at 110 ^oC. After cooling to room temperature, the mixture was washed with D.I. water and extracted with ethyl acetate. The combined organic layer was dried by Na_2SO_4, filtered and concentrated. After purification by a silica gel column chromatography with a mixture of hexane:CH_2Cl_2 (5:1 v/v), the targeted compound was obtained as a white powder (72%).

Spectral data: MS (MALDI-TOF): *m/z* 259.14 (M^+). ^1H NMR ($CDCl_3$): δ (ppm) 8.67–8.66 (m, 1H, Ar), 7.90 (d, *J* = 8.4 Hz, 2H, Ar), 7.75–7.68 (m, 2H, Ar), 7.29 (d, *J* = 8.4 Hz, 2H, Ar), 7.22–7.19 (m, 1H, Ar), 7.10 (s, 4H, Ar), 4.00 (s, 2H, CH_2), 2.32 (s, 3H, CH_3).

Synthesis of L3

This compound was obtained using the same methodology as described in **L1** but 4-benzylphenylboronic acid (1.20 g, 5.66 mmol) and 2-chloro-4-methylpyridine (0.55 g, 4.35 mmol) were used instead. The 4-methyl-2-(4-benzylphenyl)pyridine was purified by silica gel chromatography eluting with a mixture of hexane:CH_2Cl_2 (3:1, v/v) as a pale yellow oil (66%).

Spectral data: MS (MALDI-TOF): *m/z* 259.14 (M^+). ^1H NMR ($CDCl_3$): δ (ppm) 8.52 (d, *J* = 5.6 Hz, 1H, Ar), 7.89 (d, *J* = 8.4 Hz, 2H, Ar), 7.51 (s, 1H, Ar), 7.30–7.28

(m, 4H, Ar), 7.22–7.20 (m, 3H, Ar), 7.04 (d, *J* = 5.6 Hz, 1H, Ar), 4.04 (s, 2H, CH_2), 2.40 (s, 3H, CH_3).

Synthesis of L4

This compound was obtained using the same methodology as described in **L1** but 4-benzylphenylboronic acid (1.10 g, 5.19 mmol) and 2-chloro-5-methylpyridine (0.51 g, 3.99 mmol) were used instead. The 5-methyl-2-(4-benzylphenyl)pyridine was purified by silica gel chromatography eluting with a mixture of hexane:CH_2Cl_2 (3:1, v/v) as a white powder (76%).

Spectral data: MS (MALDI-TOF): *m/z* 259.14 (M^+). ^{1}H NMR ($CDCl_3$): δ (ppm) 8.49 (s, 1H, Ar), 7.88 (d, *J* = 8.4 Hz, 2H, Ar), 7.69 (d, *J* = 8.0 Hz, 1H, Ar), 7.53 (d, *J* = 10.4 Hz, 1H, Ar), 7.31–7.25 (m, 4H, Ar), 7.20 (d, *J* = 6.8 Hz, 3H, Ar), 4.03 (s, 2H, CH_2), 2.36 (s, 3H, CH_3).

Synthesis of L5

This compound was obtained using the same methodology as described in **L1** but 2-chloro-5-trifluoromethylpyridine (0.79 g, 4.35 mmol) and 4-benzylphenylboronic acid (1.20 g, 5.66 mmol) were used instead. 5-Trifluoromethyl-2-(4-benzylphenyl)pyridine was purified by silica gel chromatography eluting with a mixture of hexane:CH_2Cl_2 (2:1, v/v) as a white powder (64%).

Spectral data: MS (MALDI-TOF): *m/z* 313.11 (M^+). ^{1}H NMR ($CDCl_3$): δ (ppm) 8.95 (s, 1H, Ar), 8.08 (d, *J* = 12.4 Hz, 2H, Ar), 7.94 (d, *J* = 2.0 Hz, 1H, Ar), 7.81 (d, *J* = 8.0 Hz, 1H, Ar), 7.37–7.32 (m, 4H, Ar), 7.32–7.24 (m, 3H, Ar), 4.08 (s, 2H, CH_2).

Table S1. Electronic excitation energies (eV) and corresponding oscillator strengths (*f*), main configurations and CI coefficients of the low-lying electronic excited states of the complex **1** calculated by TDDFT//B3LYP/GENECP based on the DFT//B3LYP/ GENECP optimized ground state geometries

	Electronic transition	**Energy [eV/nm][a]**	***f*[b]**	**Composition[c]**	**CI[d]**
Singlet	$S_0 \rightarrow S_1$	2.76/449	0.0222	H→L	0.63235
	$S_0 \rightarrow S_5$	3.17/391	0.0279	H-1→L+1	0.65534
				H-1→L	0.21324
	$S_0 \rightarrow S_{10}$	3.51/354	0.0268	H-2→L	0.57317
	$S_0 \rightarrow S_{13}$	3.64/340	0.0537	H-2→L+2	0.19555
	$S_0 \rightarrow S_{22}$	4.00/310	0.0464	H-4→L+3	0.23097
	$S_0 \rightarrow S_{24}$	4.05/306	0.0830	H-4→L+2	0.40936
				H-2→L+2	0.19317
	$S_0 \rightarrow S_{27}$	4.1762/297	0.0824	H-6→L+1	0.37976

[a] Only the selected low-lying excited states are presented. [b] Oscillator strengths. [c] Only the main configurations are presented. [d] The CI coefficients are in absolute values.

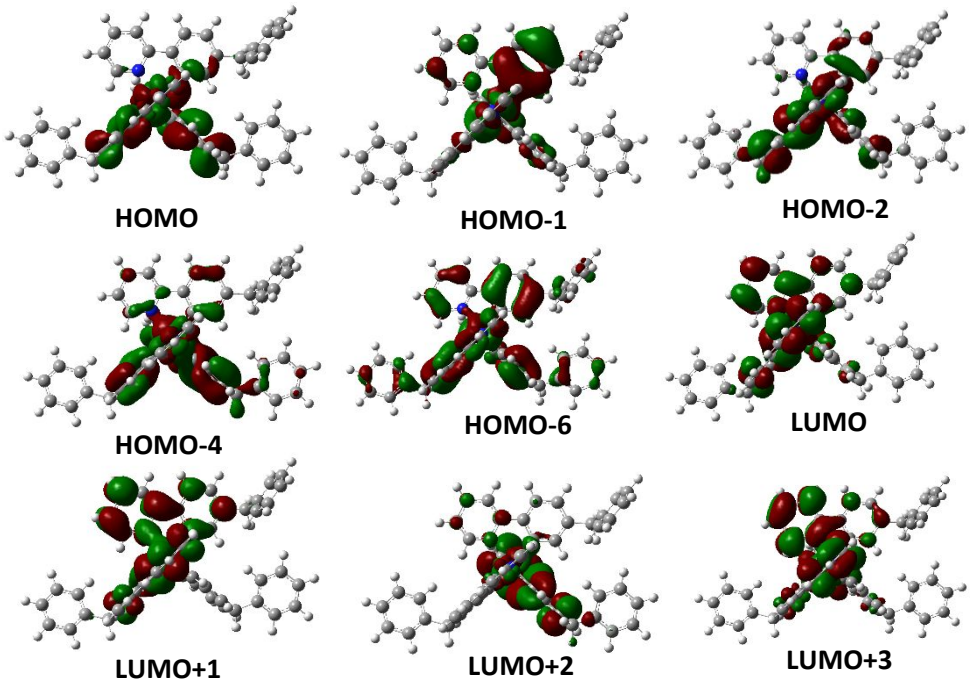

Fig. S1 Electron density maps of the frontier molecular orbital of the complex **1** based on ground state optimized geometry by the DFT calculations at the B3LYP/GENECP level with Gaussian 09W.

Table S2. Electronic excitation energies (eV) and corresponding oscillator strengths (*f*), main configurations and CI coefficients of the low-lying electronic excited states of the complex **2** calculated by TDDFT//B3LYP/GENECP based on the DFT//B3LYP/ GENECP optimized ground state geometries

	Electronic transition	**Energy [eV/nm][a]**	***f*[b]**	**Composition[c]**	**CI[d]**
Singlet	$S_0 \rightarrow S_1$	2.76/449	0.0224	H→L	0.62347
	$S_0 \rightarrow S_3$	2.93/424	0.0165	H→L+2	0.68206
	$S_0 \rightarrow S_7$	3.37/368	0.0287	H-1→L+2	0.54180
	$S_0 \rightarrow S_{13}$	3.64/341	0.0551	H-3→L	0.50437
				H-4→L	0.30676
	$S_0 \rightarrow S_{24}$	4.03/307	0.0889	H-4→L+2	0.38142
				H-3→L+3	0.12600
	$S_0 \rightarrow S_{27}$	4.16/298	0.1237	H-6→L+1	0.34567
				H-6→L	0.31726

[a] Only the selected low-lying excited states are presented. [b] Oscillator strengths. [c] Only the main configurations are presented. [d] The CI coefficients are in absolute values.

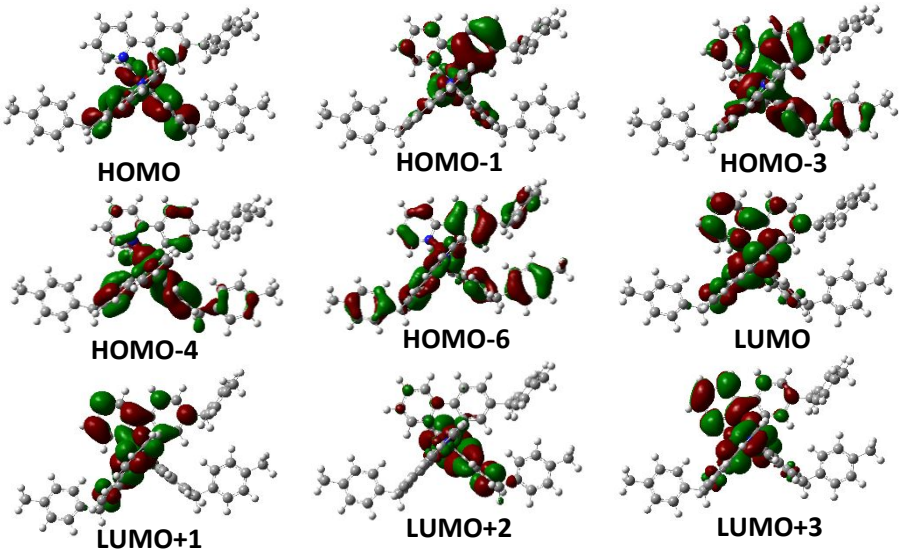

Fig. 2 Electron density maps of the frontier molecular orbital of the complex **2** based on ground state optimized geometry by the DFT calculations at the B3LYP/GENECP level with Gaussian 09W.

Table S3. Electronic excitation energies (eV) and corresponding oscillator strengths (*f*), main configurations and CI coefficients of the low-lying electronic excited states of the complex **3** calculated by TDDFT//B3LYP/GENECP based on the DFT//B3LYP/ GENECP optimized ground state geometries

	Electronic transition	**Energy [eV/nm][a]**	***f*[b]**	**Composition[c]**	**CI[d]**
Singlet	$S_0 \rightarrow S_1$	2.83/438	0.0268	H→L	0.66255
	$S_0 \rightarrow S_3$	2.96/418	0.0155	H→L+2	0.68284
	$S_0 \rightarrow S_4$	3.18/390	0.0351	H-1→L	0.68407
	$S_0 \rightarrow S_{13}$	3.66/338	0.0399	H-3→L	0.48312
				H-2→L+2	0.26565
	$S_0 \rightarrow S_{18}$	3.84/322	0.0559	H-3→L+2	0.44683
				H-2→L+2	0.31953
	$S_0 \rightarrow S_{23}$	4.07/304	0.0620	H-4→L+2	0.45614
	$S_0 \rightarrow S_{27}$	4.21/295	0.0740	H-6→L+1	0.32614

[a] Only the selected low-lying excited states are presented. [b] Oscillator strengths. [c] Only the main configurations are presented. [d] The CI coefficients are in absolute values.

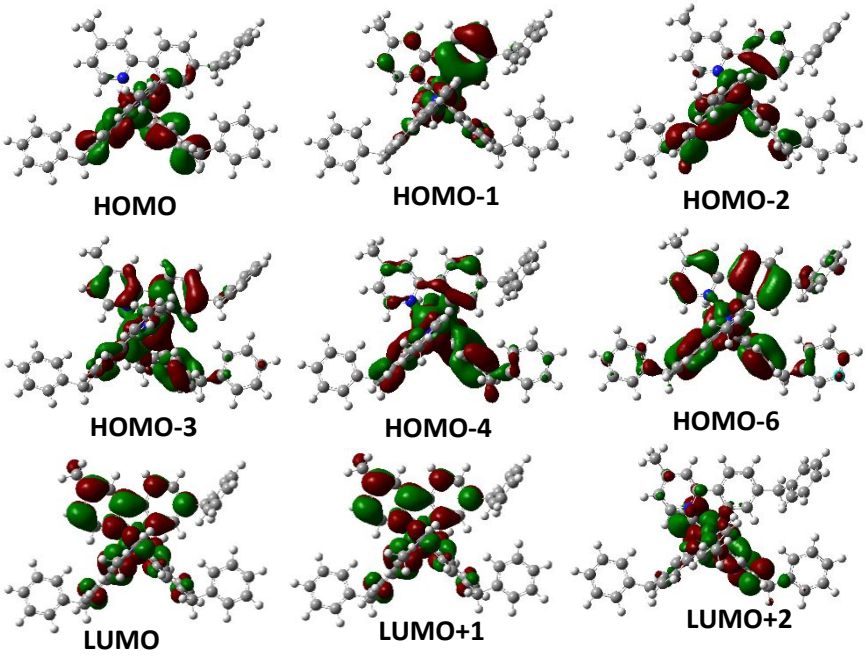

Fig. S3 Electron density maps of the frontier molecular orbital of the complex **3** Based on ground state optimized geometry by the DFT calculations at the B3LYP/GENECP level with Gaussian 09W.

Table S4. Electronic excitation energies (eV) and corresponding oscillator strengths (*f*), main configurations and CI coefficients of the low-lying electronic excited states of the complex **4** calculated by TDDFT//B3LYP/GENECP based on the DFT//B3LYP/ GENECP optimized ground state geometries

	Electronic transition	**Energy [eV/nm][a]**	***f*[b]**	**Composition[c]**	**CI[d]**
Singlet	$S_0 \rightarrow S_1$	2.76/449	0.0213	H→L	0.59737
				H→L+1	0.36140
	$S_0 \rightarrow S_3$	2.92/424	0.0176	H→L+2	0.68345
	$S_0 \rightarrow S_9$	3.43/362	0.0559	H-1→L+2	0.46236
	$S_0 \rightarrow S_{13}$	3.63/343	0.0485	H-3→L	0.51084
	$S_0 \rightarrow S_{24}$	4.01/309	0.0904	H-3→L+2	0.34895
	$S_0 \rightarrow S_{27}$	4.13/300	0.0616	H-6→L+1	0.37768
				H-2→L+5	0.27070

[a] Only the selected low-lying excited states are presented. [b] Oscillator strengths. [c] Only the main configurations are presented. [d] The CI coefficients are in absolute values.

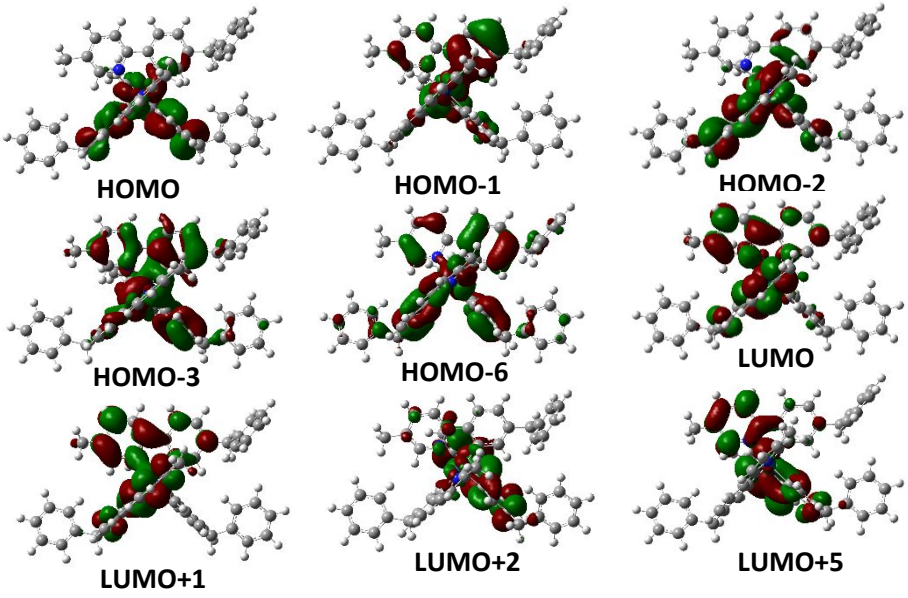

Fig. S4 Electron density maps of the frontier molecular orbital of the complex **4** based on ground state optimized geometry by the DFT calculations at the B3LYP/GENECP level with Gaussian 09W.

Table S5. Electronic excitation energies (eV) and corresponding oscillator strengths (*f*), main configurations and CI coefficients of the low-lying electronic excited states of the complex **5** calculated by TDDFT//B3LYP/GENECP based on the DFT//B3LYP/ GENECP optimized ground state geometries

	Electronic transition	**Energy [eV/nm][a]**	***f*[b]**	**Composition[c]**	**CI[d]**
Singlet	$S_0 \rightarrow S_1$	2.88/430	0.0076	H→L	0.68331
	$S_0 \rightarrow S_3$	3.14/394	0.0182	H-2→L	0.68935
	$S_0 \rightarrow S_9$	3.60/344	0.0395	H-3→L	0.46776
				H→L+4	0.42172
	$S_0 \rightarrow S_{16}$	3.93/316	0.0308	H-2→L+2	0.39441
	$S_0 \rightarrow S_{18}$	3.96/313	0.0822	H-4→L+1	0.54593
	$S_0 \rightarrow S_{27}$	4.28/289	0.2253	H-6→L+1	0.51292
				H-3→L+2	0.23942

[a] Only the selected low-lying excited states are presented. [b] Oscillator strengths. [c] Only the main configurations are presented. [d] The CI coefficients are in absolute values.

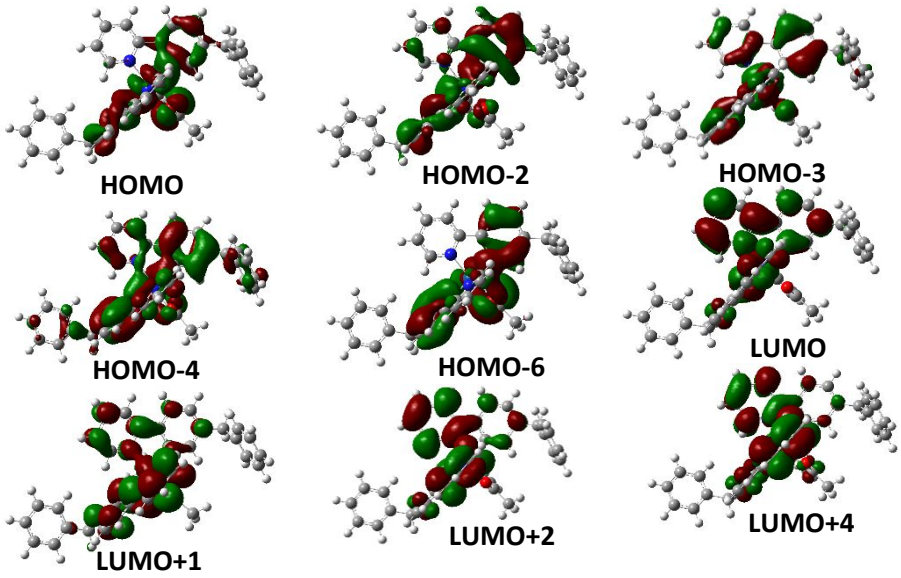

Fig. S5 Electron density maps of the frontier molecular orbital of the complex **5** based on ground state optimized geometry by the DFT calculations at the B3LYP/GENECP level with Gaussian 09W.

Table S6. Electronic excitation energies (eV) and corresponding oscillator strengths (*f*), main configurations and CI coefficients of the low-lying electronic excited states of the complex **6** calculated by TDDFT//B3LYP/GENECP based on the DFT//B3LYP/ GENECP optimized ground state geometries

	Electronic transition	**Energy [eV/nm][a]**	***f*[b]**	**Composition[c]**	**CI[d]**
Singlet	$S_0 \rightarrow S_1$	2.89/429	0.0072	H→L	0.68400
	$S_0 \rightarrow S_3$	3.15/393	0.0215	H-1→L	0.68910
	$S_0 \rightarrow S_9$	3.61/344	0.0363	H→L+4	0.46524
	$S_0 \rightarrow S_{18}$	3.95/314	0.0928	H-4→L+2	0.56995
	$S_0 \rightarrow S_{20}$	4.01/309	0.0334	H-5→L	0.46970
	$S_0 \rightarrow S_{27}$	4.27/291	0.1741	H-6→L+1	0.56997

[a] Only the selected low-lying excited states are presented. [b] Oscillator strengths. [c] Only the main configurations are presented. [d] The CI coefficients are in absolute values.

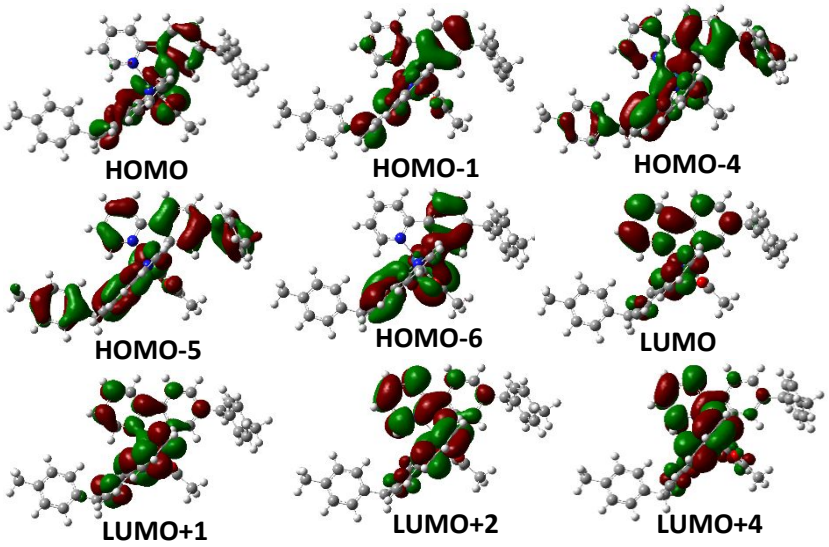

Fig. S6 Electron density maps of the frontier molecular orbital of the complex **6** based on ground state optimized geometry by the DFT calculations at the B3LYP/GENECP level with Gaussian 09W.

Table S7. Electronic excitation energies (eV) and corresponding oscillator strengths (*f*), main configurations and CI coefficients of the low-lying electronic excited states of the complex **7** calculated by TDDFT//B3LYP/GENECP based on the DFT//B3LYP/ GENECP optimized ground state geometries

	Electronic transition	**Energy [eV/nm][a]**	***f*[b]**	**Composition[c]**	**CI[d]**
Singlet	$S_0 \rightarrow S_1$	2.90/427	0.0088	H→L	0.68068
	$S_0 \rightarrow S_3$	3.17/392	0.0209	H-1→L	0.68903
	$S_0 \rightarrow S_9$	3.61/343	0.0781	H-2→L	0.63745
	$S_0 \rightarrow S_{19}$	4.00/310	0.0524	H-4→L+1	0.39485
				H-2→L+2	0.28300
	$S_0 \rightarrow S_{23}$	4.17/297	0.0463	H-5→L+1	0.55766
	$S_0 \rightarrow S_{27}$	4.30/288	0.2523	H-3→L+2	0.24657
				H-5→L	0.22219

[a] Only the selected low-lying excited states are presented. [b]Oscillator strengths. [c]Only the main configurations are presented. [d] The CI coefficients are in absolute values.

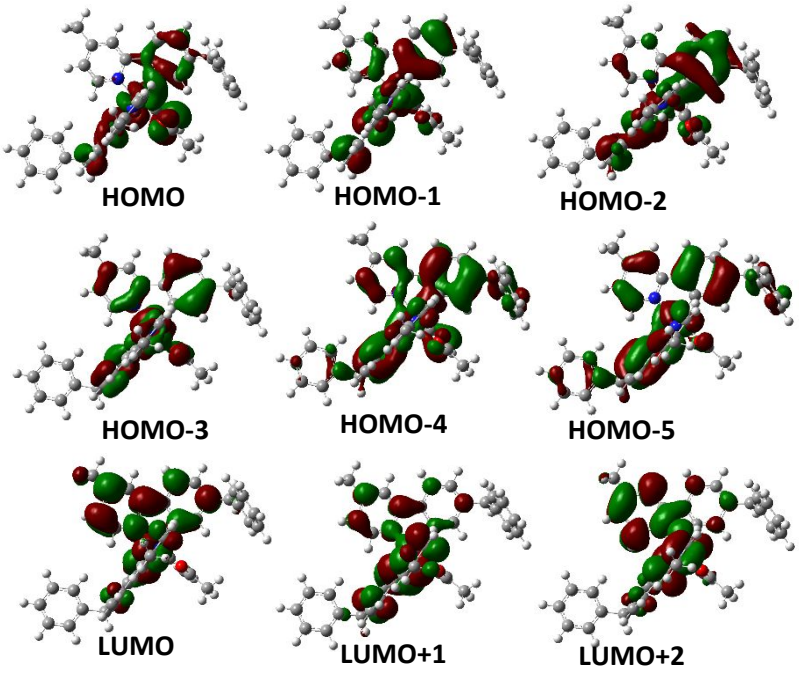

Fig. S7 Electron density maps of the frontier molecular orbital of the complex **7** based on ground state optimized geometry by the DFT calculations at the B3LYP/GENECP level with Gaussian 09W.

Table S8. Electronic excitation energies (eV) and corresponding oscillator strengths (*f*) main configurations and CI coefficients of the low-lying electronic excited states of the complex **8** calculated by TDDFT//B3LYP/GENECP based on the DFT//B3LYP/ GENECP optimized ground state geometries

	Electronic transition	**Energy [eV/nm][a]**	***f*[b]**	**Composition[c]**	**CI[d]**
Singlet	$S_0 \rightarrow S_1$	2.88/431	0.0079	H→L	0.68835
	$S_0 \rightarrow S_3$	3.15/393	0.0216	H-1→L	0.68890
	$S_0 \rightarrow S_9$	3.61/343	0.0641	H-3→L	0.60544
	$S_0 \rightarrow S_{17}$	3.96/313	0.0364	H-2→L+2	0.33306
	$S_0 \rightarrow S_{20}$	4.03/308	0.0772	H-5→L	0.45695
	$S_0 \rightarrow S_{27}$	4.29/289	0.1994	H-6→L+1	0.54541
				H-3→L+2	0.23368

[a] Only the selected low-lying excited states are presented. [b] Oscillator strengths. [c] Only the main configurations are presented. [d] The CI coefficients are in absolute values.

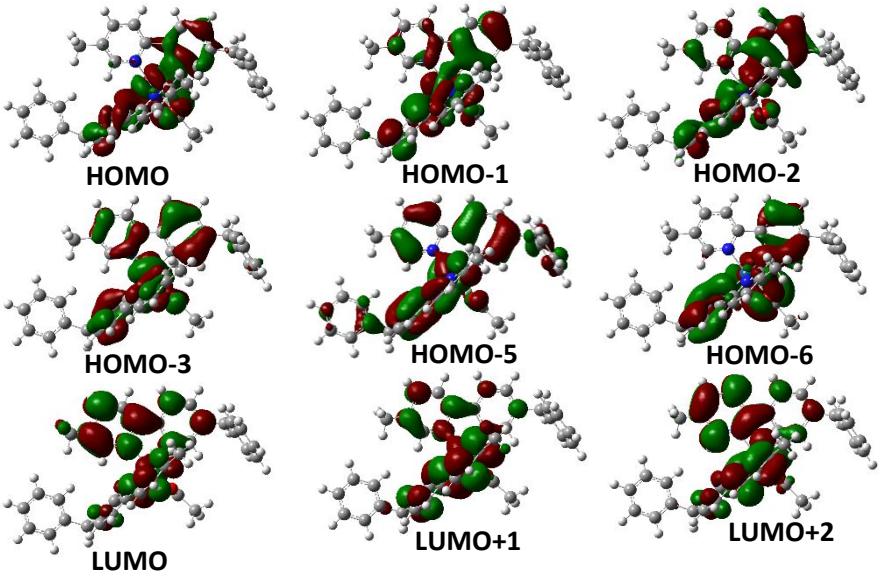

Fig. S8 Electron density maps of the frontier molecular orbital of the complex **8** based on ground state optimized geometry by the DFT calculations at the B3LYP/GENECP level with Gaussian 09W.

Table S9. Electronic excitation energies (eV) and corresponding oscillator strengths (*f*), main configurations and CI coefficients of the low-lying electronic excited states of the complex **9** calculated by TDDFT//B3LYP/GENECP based on the DFT//B3LYP/ GENECP optimized ground state geometries

	Electronic transition	**Energy [eV/nm][a]**	***f*[b]**	**Composition[c]**	**CI[d]**
Singlet	$S_0 \rightarrow S_1$	2.63/471	0.0066	H→L	0.70106
	$S_0 \rightarrow S_3$	3.01/412	0.0267	H-1→L	0.69151
	$S_0 \rightarrow S_{10}$	3.45/360	0.0761	H-3→L	0.60845
				H-1→L+2	0.20766
	$S_0 \rightarrow S_{16}$	3.77/329	0.0781	H-4→L+1	0.58668
				H-3→L+2	0.20620
	$S_0 \rightarrow S_{23}$	4.00/310	0.0711	H-6→L+1	0.39779
				H-5→L	0.26333
	$S_0 \rightarrow S_{28}$	4.14/300	0.0117	H-4→L+2	0.44028

[a] Only the selected low-lying excited states are presented. [b] Oscillator strengths. [c] Only the main configurations are presented. [d] The CI coefficients are in absolute values.

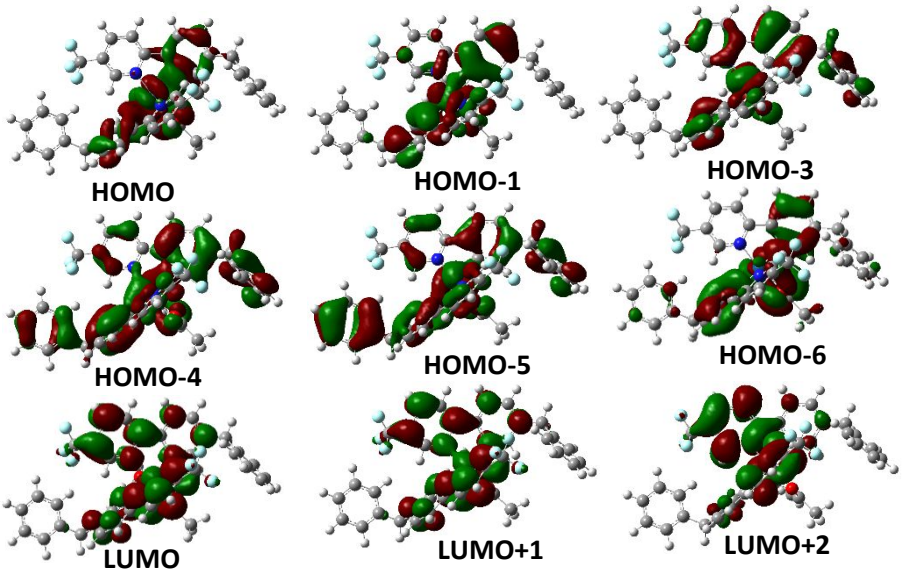

Fig. S9 Electron density maps of the frontier molecular orbital of the complex **9** based on ground state optimized geometry by the DFT calculations at the B3LYP/GENECP level with Gaussian 09W.

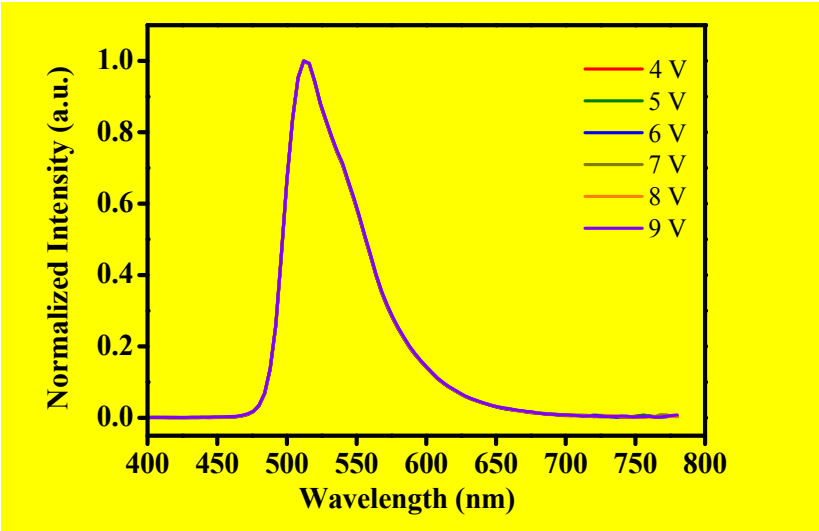

Fig. S10 Voltage independent EL spectra of **4**.

References:

1. S. J. Liu, Q. Zhao, Q. L. Fan and W. Huang, *Eur. J. Inorg. Chem.*, 2008, **13**, 2177.
2. R. S. Ashraf, M. Shahid, E. Klemm, M. Al-Ibrahim, S. Sensfuss, *Macromol. Rapid. Commun.*, 2006, **27**, 1454.

Table of Content

Highly efficient iridium(III) phosphors with 2-(4-benzylphenyl)pyridine-type ligand and their high-performance organic light-emitting diodes

Wai-Yeung Wong,* Nga-Yuen Chau, Qiwei Wang, Lu Jiang, Junlong Li and Dongge Ma*

Benzyl-modified iridium(III)-ppy electrophosphors (Hppy = 2-phenylpyridine) are synthesized and characterized. They show much improved device performance as compared to the benchmark green emitters *fac*-Ir(ppy)$_3$ and Ir(ppy)$_2$(acac) in OLEDs.

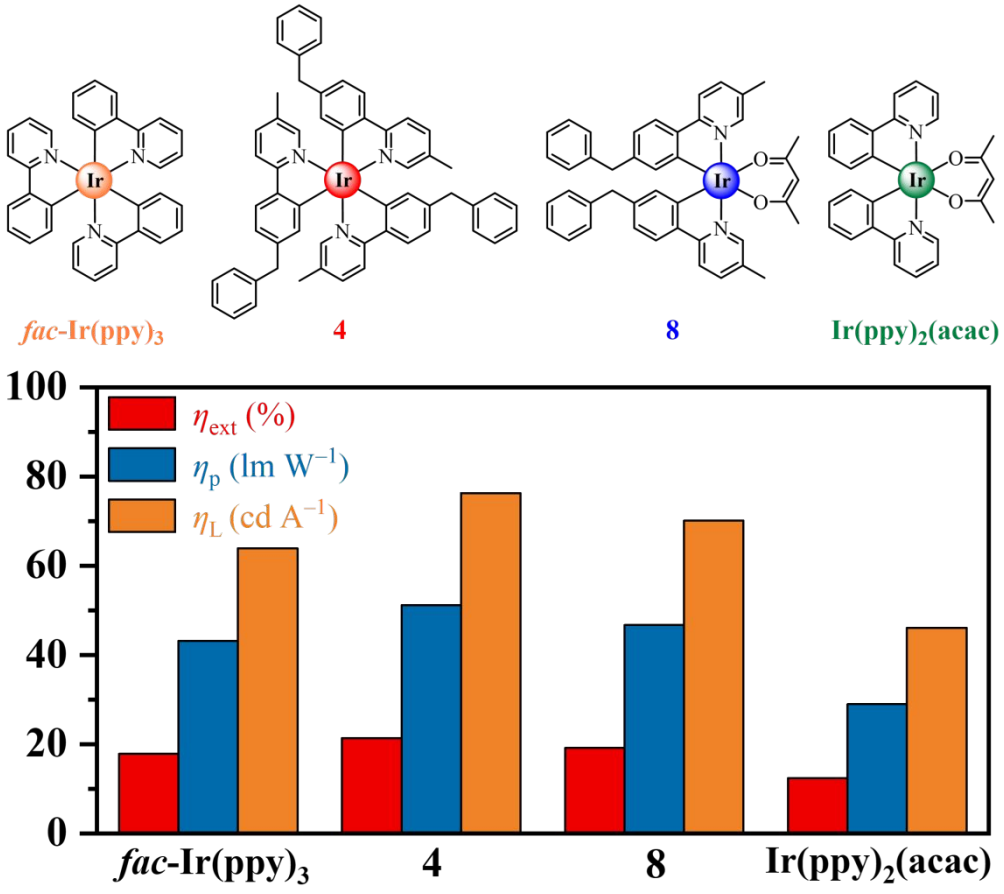

Data availability statements

The data supporting this article have been included as part of the Supplementary Information. The data that support the findings of this study are available from the corresponding author upon reasonable request.